The Karlsruhe Extensive Air Shower Simulation Code CORSIKA

J. N. Capdevielle, P. Gabriel, H. J. Gils, P. Grieder,
D. Heck, J. Knapp, H. J. Mayer, J. Oehlschläger,
H. Rebel, G. Schatz, T. Thouw
Institut für Kernphysik

Kernforschungszentrum Karlsruhe

KERNFORSCHUNGSZENTRUM KARLSRUHE

Institut für Kernphysik

KfK 4998

The Karlsruhe Extensive Air Shower Simulation Code CORSIKA

J.N. Capdevielle[1], P. Gabriel, H.J. Gils, P. Grieder[2], D. Heck,
J. Knapp[3], H.J. Mayer, J. Oehlschläger, H. Rebel, G. Schatz, T. Thouw

KERNFORSCHUNGSZENTRUM KARLSRUHE GMBH, KARLSRUHE

[1] Laboratoire de Physique Théorique, Université de Bordeaux, F-33170 Gradignan, France
[2] Physikalisches Institut der Universität Bern, CH-3012 Bern, Switzerland
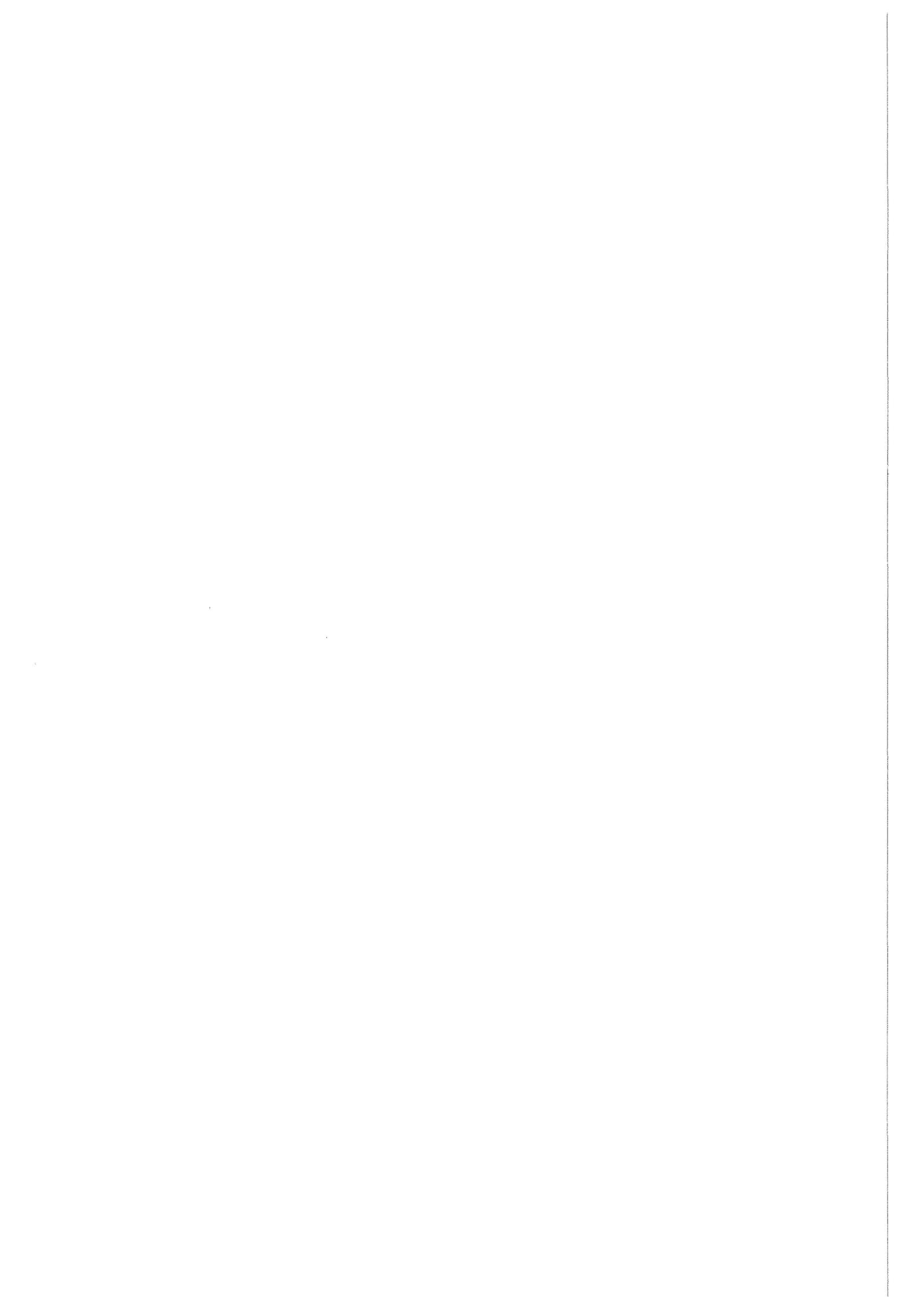[3] Institut für Experimentelle Kernphysik, Universität Karlsruhe, D-7500 Karlsruhe, Germany

Abstract

The Karlsruhe Extensive Air Shower Simulation Code CORSIKA

CORSIKA is a detailed simulation program for extensive air showers initiated by high energy cosmic particles. Primary protons and nuclei up to iron can be treated as well as photons. The reaction model for the hadronic interactions is based on the Dual Parton Model and relies on experimental data wherever possible. For electromagnetic interactions the shower program EGS4 may be used.

Zusammenfassung

CORSIKA, das Karlsruher Programm zur Luftschauersimulation

CORSIKA ist ein Programm zur detaillierten Simulation von ausgedehnten Luftschauern, die durch hochenergetische kosmische Strahlung ausgelöst werden. Wechselwirkungen von Protonen, Kernen und Photonen mit den Kernen der Atmosphäre können simuliert werden. Das Modell für die hadronischen Wechselwirkungen basiert auf dem Dual Parton Modell und orientiert sich an experimentellen Daten, wo immer das möglich ist. Elektromagnetische Prozesse können mit dem Schauerprogramm EGS4 behandelt werden.

Contents

Preface

Analyzing experimental data on Extensive Air Showers (EAS) or planning corresponding experiments requires a detailed theoretical modelling of the cascade which develops when a high energy primary particle enters the atmosphere. This can only be achieved by detailed Monte Carlo calculations taking into account all knowledge of high energy strong and electromagnetic interactions. Therefore, a number of computer programs have been written to simulate the development of EAS in the atmosphere and a considerable number of publications exists discussing the results of such calculations. A common feature of all these publications is that it is difficult, if not impossible, to ascertain in detail which assumptions have been made in the programs for the interaction models, which approximations have been employed to reduce computer time, how experimental data have been converted into the unmeasured quantities required in the calculations (such as nucleus–nucleus cross sections, e.g.) etc. This is the more embarrassing, since our knowledge of high energy interactions – though much better today than ten years ago – is still incomplete in important features. This makes results from different groups difficult to compare, to say the least. In addition, the relevant programs are of a considerable size which – as experience shows – makes programming errors almost unavoidable, in spite of all undoubted efforts of the authors. We therefore feel that further progress in the field of EAS simulation will only be achieved, if the groups engaged in this work make their programs available to (and, hence, checkable by) other colleagues. This procedure has been adopted in high energy physics and has proved to be very successful. It is in the spirit of these remarks that we want to describe in this report the physics underlying the CORSIKA program developed during the last few years by a combined Bern–Bordeaux–Karlsruhe effort. We also plan to publish a listing of the program as soon as some more checks of computational and programming details have been performed. We invite all colleagues interested in EAS simulation to propose improvements, point out errors or bring forward reservations concerning assumptions or approximations which we have made. We feel that this is a necessary next step to improve our understanding of EAS.

Chapter 1

Introduction

CORSIKA (COsmic Ray SImulations for KAscade) is a detailed Monte Carlo program to study the evolution of EAS in the atmosphere initiated by photons, protons or nuclei of energies up to 10^{17} eV. It was developed to perform simulations for the KASCADE experiment [1] presently under construction at Karlsruhe. Wherever possible experimentally accessible data have been used as a basis for modelling the high energy interactions of particles with the nuclei of the atmosphere. All secondary particles are tracked explicitly along their trajectories and their parameters are stored on tape when reaching an observation level. This allows a detailed analysis of all features of the simulated showers.

The CORSIKA code has been developed on the basis of three well established program systems. The first was written in the 1970s by P.K.F. Grieder [2] and treats the hadronic part of proton induced showers using fire ball and isobar models. Its general program structure has been adopted in CORSIKA and the interaction routines of this program are used for the hadronic interactions at low energies. The second program was developed by J.N. Capdevielle [3] following the Dual Parton Model (DPM) [4]. It describes the hadronic interactions of protons at high energies in good agreement with the measured collider data. For simulating the electromagnetic part of an air shower we incorporated the code EGS4 [5] used successfully in the detector simulation of particle physics experiments. It was slightly modified to the requirements of air shower simulations.

These three programs were merged together and extended by several additional features. The hadronic interaction model is complemented to treat primary nuclei as well. The fraction of interacting nucleons in target and projectile are taken into account. The fragmentation of nuclei in a collision can be calculated in two different ways. Diffractive and charge exchange reactions are implemented. The photoproduction of muon pairs and hadrons is added to the electromagnetic part to allow the calculation of the muon content of photon induced showers. A second way of treating the electromagnetic component is to use the corrected and adapted form [6, 7] of the analytic NKG formula for each electron or photon produced in the hadronic cascade. It allows to study the longitudinal development of the electromagnetic cascade and the electron density at particular coordinates at the observation level.

This option is added to CORSIKA to allow a fast but less accurate simulation of hadronic showers. The density variation of the atmosphere with altitude and its elemental composition are included.

With this program many calculations have been performed with p, α, O, Fe and γ primaries in an energy range of $10^{12}\ eV \leq E_0 \leq 10^{17}\ eV$. Particle numbers for electrons, muons and hadrons, their lateral and energy distributions, arrival times and many other features have been evaluated from the simulations and compared with experimental data, where available. The agreement gives us confidence to have with CORSIKA a useful and flexible tool to study cosmic rays and their secondaries at high primary energies.

The scope of this report is a description of the physical basis and the parametrizations actually used in CORSIKA and to show its capabilities and limitations. The program is in permanent modification by improvements and further details. This report refers to the actual version [1]. Most recent changes, however, were shown to have minor effects on the global features of simulated showers.

---

[1] Version 3.05 released in March 92

Chapter 2

Program frame

2.1 Control and run

At the beginning of the simulation a variety of parameters can be chosen to control the simulation. The primary particle type and its angle of incidence have to be defined. The primary energy can be prechosen or selected at random in a particular energy range with a given slope of the energy spectrum. This allows a realistic simulation of the steeply falling shower rate with rising energy. Up to 10 observation levels can be defined and data on all particles penetrating these levels are recorded as long as the energy exceeds a cut–off specified for hadrons, muons, electrons, or photons separately. Several flags control the hadronic interaction model at high energies (see section 6.1) and two flags switch on or off the two options for the simulation of electromagnetic cascades (see section 6.3).

2.2 Particles

The CORSIKA program recognizes 16 elementary particles. These are γ, $e^{\pm}$, $\mu^{\pm}$, π^{0}, $\pi^{\pm}$, $K^{0}_{S/L}$, $K^{\pm}$, p, n, $\bar{p}$, and $\bar{n}$. In addition nuclei up to $A = 56$ can be treated. They are defined them by their numbers of protons and neutrons. All these particles can be tracked through the atmosphere, are able to interact, annihilate or decay and produce secondary particles. They are fully defined in the program by their particle identification, the Lorentz factor, the zenith and azimuthal angle of the trajectory, the time since the first interaction of the primary, and the three spatial coordinates x, y and z. The number of inelastic hadronic reactions or decays which the parent particles have suffered is protocolled as the generation of a particle. The particle masses are stored in an array for fast access during the calculations. Particle identifiers and masses of elementary particles are taken from the GEANT 3 detector Monte Carlo code [8]. Nuclear masses are calculated according to the Bethe-Weizsäcker formula. For nuclei with $Z < 15$ the mass is set to the mass of the most abundant isotope. Some short–lived particles like η, ρ, Σ, or Λ are taken into account as intermediate stages of particle production without appearing as explicit

5

Layer i	Altitude h (km)	a_i (g/cm^2)	b_i (g/cm^2)	c_i (cm)
1	$0\ldots4$	-186.5562	1222.6562	994186.38
2	$4\ldots10$	-94.919	1144.9069	878153.55
3	$10\ldots40$	0.61289	1305.5948	636143.04
4	$40\ldots100$	0.0	540.1778	772170.16
5	>100	0.01128292	1	10^9

Table 2.1: Parameters of the atmospheric model.

particles in the cascade. Neutrinos from π, μ, and K decays are discarded.

2.3 Coordinate system

The coordinates in CORSIKA are defined with respect to a Cartesian coordinate system with the positive x–axis pointing to the magnetic north, the positive y–axis to the west, and the z–axis upwards. The origin is located at sea level. This definition is necessary, because the earth's magnetic field is taken into account. It is implemented for the location of Karlsruhe ($49°$ N, $8°$ E) as described in section 4.3. The zenith angle Θ of a particle trajectory is measured between the particle momentum vector and the negative z–axis, and the azimuthal angle ϕ between the positive x–axis and the x-y–component of the particle momentum vector (i.e. with respect to north) proceeding counterclockwise.

2.4 Atmosphere

The atmosphere adopted consists of N_2, O_2, and Ar with the volume fractions of 78.1%, 21.0%, and 0.9% [9]. The density variation of the atmosphere with altitude is parametrized according to J. Linsley [10] following the U.S. standard atmosphere. This model is composed of 5 layers. In the lower four of them the density follows an exponential dependence on the altitude leading to a relation between the mass overburden $T(h)$ of the atmosphere and the height h of the form

$$T(h) = a_i + b_i \cdot e^{-h/c_i} \qquad i = 1, \ldots 4 \quad . \tag{2.1}$$

In the fifth layer the mass overburden decreases linearly with height

$$T(h) = a_5 - b_5 \cdot h/c_5 \quad .$$

The boundary of the atmosphere in this model is defined at the height where the mass overburden $T(h)$ vanishes, which is at $h = 112.8$ km. The parameters are listed in table 2.1.

The passage of the primary particle through the atmosphere starts at the upper border of the atmospheric model. From this starting point the place of the first interaction is calculated. The coordinates of the point of first interaction are set to $(0, 0, z_0)$. At each observation level the x and y coordinates are shifted such that the shower axis retains the coordinates $(0, 0, z_{obs})$. This is done to facilitate later analysis.

2.5 Random number generator

The Monte Carlo method is essentially based on random numbers and, hence, a random number generator that meets the requirements of the today's increasingly long and complex calculations is indispensible. CORSIKA is operated with the random number generator RANMAR [11] in the version as implemented in the CERN program library [12] which represents the state of the art in computational physics. It is a pseudo random number generator delivering uniformly distributed numbers. It offers the possibility to generate simultaneously up to $9 \cdot 10^8$ independent sequences with a sequence length of $\approx 2 \cdot 10^{44}$ each. The generator is written in standard FORTRAN and, thus, portable to all other computers where bit–identical results are obtained. It satisfies very stringent tests on randomness and uniformity, and it is sufficiently fast.
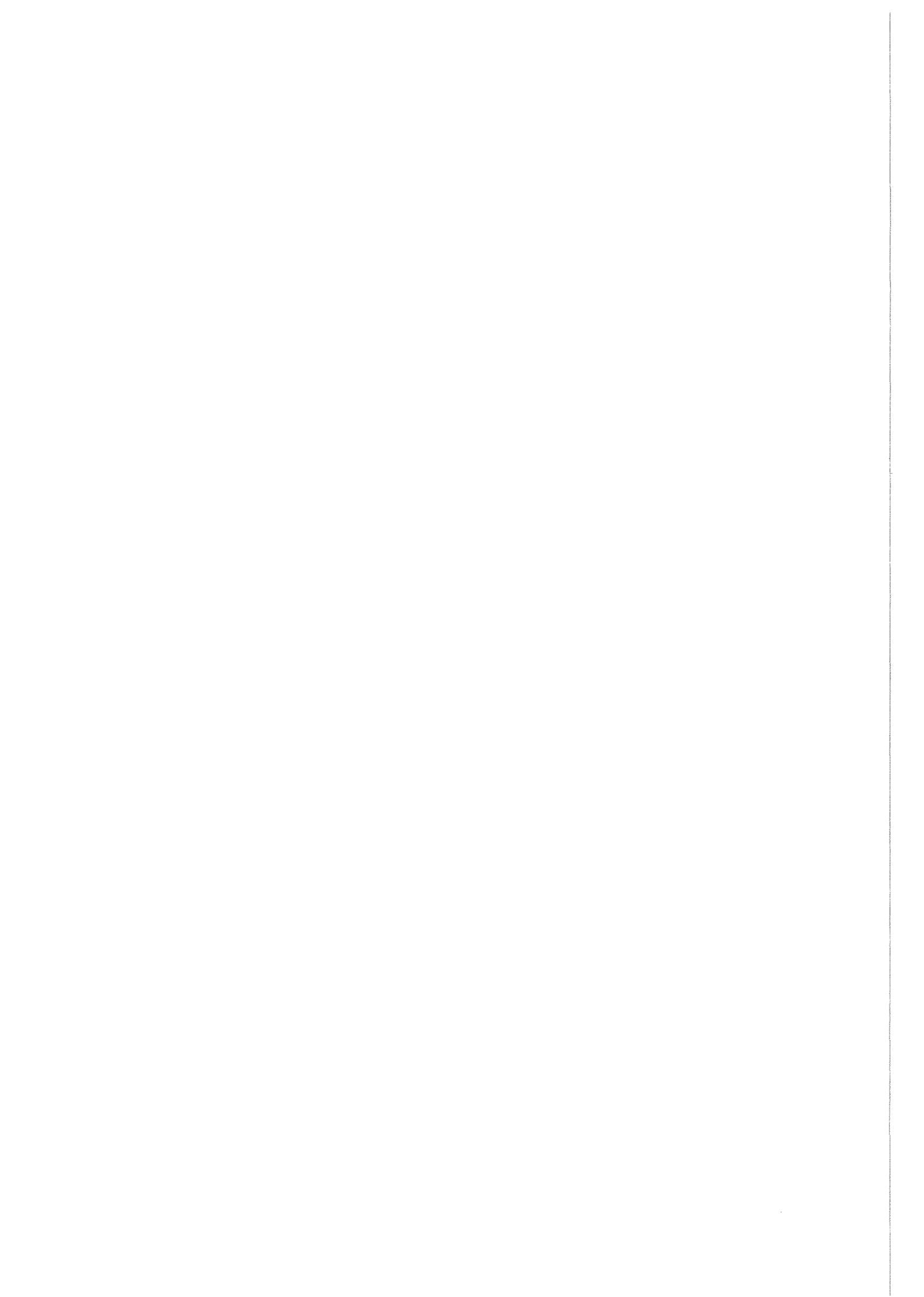
Chapter 3

Mean free path

The distance a particle travels before it undergoes its next inelastic interaction or decay is determined by the cross section for a hadronic reaction and the probability to decay. Stable particles can only interact, for unstable ones the two processes compete and are considered independently. Electrons and photons are treated in the EGS4 routines. A description of the processes they may suffer can be found in [5].

3.1 Muons

Muons are assumed to propagate without undergoing nuclear reactions, thus only decay determines the path length ℓ of a muon. Its mean is defined by

$$\ell_D = c \cdot \tau_\mu \cdot \gamma_\mu \cdot \beta_\mu$$

where c is the vacuum speed of light, τ_μ is the muon lifetime at rest, γ_μ is its Lorentz factor and β_μ its velocity in units of c. The probability of a muon to travel the distance ℓ before it decays is then

$$P_D(\ell) = \frac{1}{\ell_D} \cdot e^{-\ell/\ell_D}$$

and the path length of a muon is chosen at random from this distribution. It should be noted that in the above formulas ℓ has the dimension of cm. The path lengths are expressed in units of g/cm^2 by taking into account the actual density and its variation along the trajectory. For a given path length ℓ in cm one obtains the path length λ in g/cm^2 as

$$\lambda = f(\ell, h, \theta) = \frac{T(h_2) - T(h_1)}{\cos(\theta)}$$

with $h_2 = h_1 - \ell \cdot \cos(\theta)$. It depends on the altitude of its origin h_1 and the direction of propagation. $T(h)$ is given by eq. 2.1. The probability distribution for the decay

9

distance λ in g/cm^2 is then

$$P_D(\lambda) = P_D(\ell) \cdot \frac{d\ell}{d\lambda} = P(f^{-1}(\lambda)) \cdot \frac{df^{-1}(\lambda)}{d\lambda} \qquad (3.1)$$

where f^{-1} represents the inverse function of f.

3.2 Nucleons and nuclei

3.2.1 Nucleon–nucleon cross section

The free path of nucleons as stable particles is determined by their inelastic nucleon–nucleon cross section only. This cross section is experimentally available for nucleon laboratory momenta p up to 1000 GeV/c [13] which corresponds to a center of mass (cm) energy of 44.7 GeV. The measurements can well be parametrized as

$$\sigma_{n-n}(p) = A + B \cdot p^N + C \cdot \log^2 p + D \cdot \log p \qquad (3.2)$$

where A, B, C, D, and N are free parameters of the fit. Their values are given in table 3.1. For larger momenta the cross section is extrapolated by

$$\sigma_{n-n}(p) = 22.01 \cdot (p_{lab}^2 + m^2)^{0.0321} \qquad (3.3)$$

where p is given in GeV/c and σ_{n-n} is in mb. This represents an empirical fit to the proton–antiproton inelastic cross section which is known up to 1800 GeV cm energy and which is expected to be equal to the nucleon–nucleon cross section at these energies.

Above 1000 GeV/c, we will follow the extrapolation resulting from the DPM [14] taken as

$$\sigma_{p-p}^{inel.}(p) = 0.314 \cdot \log^{1.8} s + 23 \quad . \qquad (3.4)$$

At low energies the measured inelastic cross section drops rapidly. Below $p_{lab} = 10\ GeV/c$ only elastic reactions with a constant cross section of

$$\sigma_{n-n}(p = 10\ GeV/c) = 29.9\ mb$$

are allowed. For antinucleons annihilation with nucleons can occur in addition, leading to a contribution to the inelastic cross section which is parametrized in ref. [13] by

$$\sigma_{an}(p) = 0.532 + 63.4 \cdot p^{-0.71} \quad . \qquad (3.5)$$

10

Param.	$N - N$	$\pi - N$	$K - N$
A	30.9	24.3	12.3
B	-28.9	-12.3	-7.77
C	0.192	0.324	0.0326
D	-0.835	-2.44	0.738
N	-2.46	-1.91	-2.12

Table 3.1: Parameters of the hadron–nucleon cross section parametrization.

3.2.2 Nucleus–nucleus cross section

In EAS nucleons or complex nuclei are reacting with air nuclei. In the energy range of interest no experimental data exist on the relevant quantities, such as inelastic cross section and number of target and projectile nucleons participating in the reaction. So they have to be calculated from the nucleon–nucleon cross section following Glauber theory [15, 16]. The input nucleon distributions of nuclei are derived from measured charge distributions [17] unfolding the finite size of the proton with a ms charge radius of $\langle r_p^2 \rangle^{1/2} = 0.862 \, fm$. For nuclei below mass number 20 the charge distributions are assumed to be Gaussian and the radius of the nucleon distribution is

$$\langle r_m \rangle^2 = \langle r_{ch} \rangle^2 - \langle r_p \rangle^2 \quad .$$

For $A > 20$ the charge distributions are approximated by the Fermi function. Unfolding was done by folding a correspondingly parametrized nucleon distribution with the proton charge distribution to obtain the measured radius and slope of the charge distribution of the nucleus. From the Glauber method the inelastic cross section for 40 projectile nuclei with $A = 1 \ldots 56$ colliding with the target nuclei ^{14}N, ^{16}O, and ^{40}Ar were calculated for three different values of the nucleon–nucleon cross section (30, 45 and 60 mb corresponding to nucleon–nucleon collisions at laboratory energies of 120 GeV, 66.5 TeV, and 5.87 PeV, respectively). In addition, the probability of n_P projectile nucleons interacting and the probability of a projectile nucleon hitting n_T target nucleons were evaluated. Values for mass numbers for which no experimental charge distributions were available have been interpolated. The results are tabulated in CORSIKA and between the table values a quadratic interpolation is performed with respect to σ_{n-n} to obtain intermediate values of the cross section σ_{N-air} of a nucleon or nucleus with air.

The interaction mean free path λ_I is obtained by

$$\lambda_I = m_{air} / \sigma_{N-air}$$

where $m_{air} = 14.54 \, amu$ is the mass of an average atom of air in g and λ_I is given here in g/cm^2. The probability of the projectile to traverse a layer of atmosphere of

11

the thickness λ without interaction is then

$$P_I(\lambda) = \frac{1}{\lambda_I} \cdot e^{-\lambda/\lambda_I} \quad .$$

According to this distribution, the path lengths of nucleons and nuclei are chosen at random.

3.3 Pions and kaons

Neutral pions are subject to a special treatment as compared to charged pions or kaons. Due to their short lifetime, they decay nearly at their creation point. Therefore, π^0s are not tracked at all but decay immediately.

In contrast, charged pions and kaons are particles where decay and nuclear interaction compete. Their decay lengths are determined in the same way as for muons just replacing the free muon lifetime τ_μ by the pion and kaon lifetimes τ_π and τ_K, respectively.

Their interaction lengths are treated in analogy to those of nucleons. Existing measurements of $\pi - N$ and $K - N$ reactions show a similar dependence on the momentum p as nucleons. Therefore, eq. 3.2 can be fitted to the measured π and K data as well. The results of such fits have been taken from ref. [13] and are listed in table 3.1. In the momentum region above 1000 GeV/c the cross sections for π and K are assumed to rise with the same momentum dependence as for nucleons. In order to get a continuous transition between the two energy regimes, only the scaling factors were modified compared to the nucleon case in eq. 3.3.

$$\begin{aligned}
\sigma_{\pi-N}(p) &= 14.70 \cdot (p_{lab}^2 + m^2)^{0.0321} \\
\sigma_{K-N}(p) &= 12.17 \cdot (p_{lab}^2 + m^2)^{0.0321} \quad .
\end{aligned}$$

Again the cross sections are taken to be constant below $p_{lab} = 5$ GeV/c for pions and $p_{lab} = 10$ GeV/c for kaons to account for elastic scattering in this energy region. The used cross section values are

$$\begin{aligned}
\sigma_{\pi-n}(p = 5 \ GeV/c) &= 20.64 \ mb \\
\sigma_{K-n}(p = 10 \ GeV/c) &= 14.11 \ mb \quad .
\end{aligned}$$

The free path in presence of decay and interaction is evaluated by selecting at random a decay length and an interaction length independently and taking the smaller one as the actual path length. By this procedure it is also decided, whether a particle decays or interacts.

12

Chapter 4

Particle tracking

For propagating particles between two interaction points their space and time coordinates as well as their energy have to be updated. For electrons and photons this is done in EGS4 as described in ref. [5] and section 6.3.1. Charged particles lose energy by ionization, whereas neutral particles proceed without energy loss. For $\mu^\pm$ a deflection due to multiple Coulomb scattering is taken into account. This is neglected for charged hadrons. All charged particle trajectories are bent in the earth's magnetic field. The time update is handled for all particles in the same straight forward way. If particles cross an observation level while being tracked to the next interaction point, their space, momentum, and time coordinates are computed for the observation level and transferred to the particle output file.

4.1   Ionization energy loss

The ionization loss of a charged particle which traverses matter of thickness λ equals

$$dE = \frac{\kappa \cdot \lambda}{\beta^2} = \frac{\gamma^2 \cdot \kappa \cdot \lambda}{\gamma^2 - 1}$$

where $\beta = v/c$ is the velocity of the particle in the laboratory in units of the velocity of light, and γ is its Lorentz factor. The specific ionization loss in air for minimum ionizing particles is $\kappa = 2\ MeV/gcm^{-2}$. The above expression is used to compute the ionization losses along the trajectory of the particle.

Whenever, after updating the energy, the corresponding Lorentz factor is below the cut-off value, the particle is dropped from the calculation.

4.2   Multiple Coulomb scattering

The process of Coulomb scattering is considered at the end of each tracking step. The mean square value of the polar scattering angle θ of a given path is calculated

13

according to the expression given in ref. [18]

$$\langle \theta^2 \rangle = \lambda \cdot \theta_s^2 \qquad \text{with} \qquad \theta_s^2 = \frac{1}{\lambda_s} \cdot \left(\frac{E_s}{m \cdot \gamma \cdot \beta^2} \right)^2 \qquad .$$

Here E_s is the scattering constant ($0.021 \; GeV$), m, γ, and β represent the mass, Lorentz factor and velocity in the laboratory, respectively. λ is the amount of matter traversed by the particle and λ_s is the scattering length for Coulomb scattering in air ($37.7 \; g/cm^2$). A Gaussian distribution is introduced to account for the statistical nature of the scattering process [18]

$$P(\theta, \lambda) = \frac{1}{\sqrt{\pi \cdot \theta_s^2 \cdot \lambda}} \cdot e^{-\theta^2 / \lambda \cdot \theta_s^2} \qquad .$$

The value for θ is picked at random according to this distribution. The radial deviation from the straight trajectory is computed and the azimuthal angle is selected at random from a uniform distribution. Using these two angles, the x and y coordinates at the end point of the scattered trajectory are computed.

4.3 Deflection in the earth's magnetic field

The earth's magnetic field is characterized by its strength B_E and its inclination angle δ. In central Europe these values are

$$B_E = 47.24 \; \mu T \qquad \delta = 65° \qquad .$$

A particle with charge q and momentum $\vec{p}$ travelling along the path length ℓ in the magnetic field $\vec{B}$ suffers a deflection which points to the direction normal to the plane spanned by $\vec{B}$ and $\vec{p}$. The direction is changed by the angle α which, for small deflection angles, is approximately given by

$$\alpha \approx \ell \cdot q \cdot \frac{\vec{p} \times \vec{B}}{p^2} \qquad .$$

4.4 Time of flight

At the first interaction of the primary in the atmosphere the timing of the shower is started. The time interval dt which elapses as the particle moves along its path is computed by dividing the particular path length ℓ by the average particle velocity β_{ave}. Thus,

$$dt = \frac{\ell}{c \cdot \beta_{ave}}$$

where β_{ave} is the arithmetic mean of the laboratory velocities of the particle at beginning and end of the trajectory.

The total time elapsed since the first interaction is the sum of all time intervals accumulated by the successive particles to the particular observation level.

14

Chapter 5

Particle decays

Most of the particles produced in a high energy interaction are unstable and decay
into other stable or unstable particles. Neutral pions have such a short lifetime that
interaction is negligible before they decay. Muons are prevented from penetrating
the complete atmosphere by decay only. Neutrons are treated as stable particles
due to their long lifetime. For all the other unstable particles there is a competition
between interaction and decay processes and the decision is taken when calculating
the actual free path as described in section 3.3. In this section we describe the
treatment of particle decays in CORSIKA.

5.1 π^0 decay

Neutral pions decay predominantly into 2 photons. The Dalitz decay $\pi^0 \longrightarrow e^+e^-\gamma$
happens in 1.2% of the cases only and is neglected. The decay into two photons is
isotropic in the cm system of the π^0. There, the photon energy is $E_{\gamma cm} = m_{\pi^0}/2$
and the angle with respect to the direction of motion in the laboratory system is
θ_{cm}. In the laboratory system which moves with β_{π^0} with respect to the cm system
the energies and angles of the photons can be found by Lorentz transformation

$$E^i_{\gamma\ lab} = \frac{1}{2} \cdot \gamma_{\pi^0} \cdot m_{\pi^0} \cdot (1 \pm \beta_{\pi^0} \cdot \cos\theta_{cm})$$

$$\cos\theta^i_{lab} = \frac{\beta_{\pi^0} \pm \cos\theta_{cm}}{1 \pm \beta_{\pi^0} \cdot \cos\theta_{cm}} \qquad i = 1, 2 \quad.$$

The values of $\cos\theta_{cm}$ and the angle ϕ around the moving direction are selected at
random to get a uniform distribution over the whole solid angle.

5.2 $\pi^\pm$ decay

The decay $\pi^\pm \longrightarrow \mu^\pm + \nu_\mu$ is a two body decay isotropic in the cm system of the
pion. Therefore, $\cos\theta_{cm}$ and ϕ_{cm} of the muon are taken from a uniform distribution

15

and the energy is shared between muon and neutrino in a way that their momenta add up to zero. This leads to

$$E_{\mu\ cm} = \frac{m_\pi^2 + m_\mu^2}{2 \cdot m_\pi} = m_\mu \cdot \gamma_{\mu cm} = 1.039 \cdot m_\mu$$

and after Lorentz transformation into the laboratory system

$$\gamma_{\mu\ lab} = \gamma_\pi \cdot \left(\gamma_{\mu\ cm} + \beta_\pi \cdot \cos\theta_{\mu\ cm} \cdot \sqrt{\gamma_{\mu\ cm}^2 - 1} \right)$$

$$\cos\theta_{\mu\ lab} = \frac{\gamma_\pi \cdot \gamma_{\mu\ lab} - \gamma_{\mu\ cm}}{\gamma_\pi \cdot \beta_\pi \cdot \sqrt{\gamma_{\mu\ lab}^2 - 1}} \quad .$$

The muon carries a longitudinal polarization

$$\xi = \frac{1}{\beta_\mu} \cdot \left(\frac{E_{\pi\ lab}}{E_{\mu\ lab}} \cdot \frac{2r}{1-r} - \frac{1+r}{1-r} \right)$$

with $r = (m_\mu / m_\pi)^2$ as given in [19]. The neutrino is not tracked explicitly.

5.3 μ decay

At the end of its track, a muon can only decay via $\mu^\pm \longrightarrow e^\pm \nu_e \nu_\mu$. The electron energy distribution in the cm system is [20]

$$\frac{dN_e}{dE_{e\ cm}} \propto 3 \cdot \frac{m_\mu^2 + m_e^2}{2 \cdot m_\mu} \cdot E_{e\ cm}^2 - 2 \cdot E_{e\ cm}^3$$

from which the electron cm energy $E_{e\ cm}$ is taken at random. The direction correlation of this 3–body decay is governed by the longitudinal polarization ξ of the muon. The electron direction in the cm system is determined with the uniformly distributed angle $\cos\delta$ to be

$$\cos\theta_{cm} = \frac{\sqrt{1 + \xi \cdot A \cdot (2 \cdot \cos\delta + \xi \cdot A)} - 1}{\xi \cdot A} \quad \text{with} \quad A = \frac{1 - 2 \cdot x}{2 \cdot x - 3}$$

where x is the ratio of the electron energy to its maximum value

$$x = \frac{2 \cdot m_\mu \cdot E_{e\ cm}}{m_\mu^2 + m_e^2} \quad .$$

The Lorentz transformation into the laboratory system with the mean velocity β_μ leads to the laboratory energy and direction

$$E_{e\ lab} = m_e \cdot \gamma_{e\ lab} = \gamma_\mu \cdot \left(E_{e\ cm} + \beta_\mu \cdot p_{e\ cm} \cdot \cos\theta_{cm} \right)$$

$$\cos\theta_{lab} = \frac{\gamma_\mu}{m_e \cdot \sqrt{\gamma_{e\ lab}^2 - 1}} \cdot \left(p_{e\ cm} \cdot \cos\theta_{cm} + \beta_\mu \cdot E_{e\ cm} \right) \quad .$$

16

Decay mode	Branching ratio (%)	Decay mode	Branching ratio (%)
$K^{\pm} \longrightarrow \mu^{\pm} + \nu$	63.5	$K^0_S \longrightarrow \pi^+ + \pi^-$	68.6
$K^{\pm} \longrightarrow \pi^{\pm} + \pi^0$	21.2	$K^0_S \longrightarrow 2\pi^0$	31.4
$K^{\pm} \longrightarrow \pi^{\pm} + \pi^{\pm} + \pi^{\mp}$	5.6	$K^0_L \longrightarrow \pi^{\pm} + e^{\mp} + \nu$	38.7
$K^{\pm} \longrightarrow \pi^0 + e^{\pm} + \nu$	4.8	$K^0_L \longrightarrow \pi^{\pm} + \mu^{\mp} + \nu$	27.1
$K^{\pm} \longrightarrow \pi^0 + \mu^{\pm} + \nu$	3.2	$K^0_L \longrightarrow 3\pi^0$	21.8
$K^{\pm} \longrightarrow \pi^0 + \pi^0 + \pi^{\pm}$	1.7	$K^0_L \longrightarrow \pi^+ + \pi^- + \pi^0$	12.4

Table 5.1: Decay modes and branching ratios for kaons.

5.4 Kaon decays

Kaon decays produce a variety of final states consisting mostly of two or three particles. The dominant decays and their branching ratios are listed in table 5.1. The two body decays are isotropic in the cm system and, hence, can be treated in analogy to the pion decay (see section 5.2). The secondary particles are emitted back–to–back and their γ factors are

$$\gamma_{1\ cm} = \frac{m_K^2 + m_1^2 - m_2^2}{2 \cdot m_K \cdot m_1} \quad \text{and} \quad \gamma_{2\ cm} = \frac{m_K^2 - m_1^2 + m_2^2}{2 \cdot m_K \cdot m_2} \quad .$$

After transformation to the laboratory system, the γ factors and angles are

$$\gamma_{i\ lab} = \gamma_K \cdot \left(\gamma_{i\ cm} + \beta_K \cdot \cos\theta_{i\ cm} \cdot \sqrt{\gamma_{i\ cm}^2 - 1} \right)$$

$$\cos\theta_{i\ lab} = \frac{\gamma_K \cdot \gamma_{i\ lab} - \gamma_{i\ cm}}{\gamma_K \cdot \beta_K \cdot \sqrt{\gamma_{i\ lab}^2 - 1}} \qquad i = 1, 2 \quad .$$

The situation for the three body decays is a bit more complicated, because the particle energies in the cm system are not fixed, but vary in the kinematically allowed range. However, momentum and energy conservation restrict the three secondary particles to lie in one plane and to share the cm energy. The energies are calculated to fall inside a Dalitz plot which gives a probability density function for a decay depending on the variables p_{12}, p_{13} where $p_{ik} = p_i + p_k = -p_l$ are the sums of the momenta of the two particles. This probability density function directly depends on the matrix element $|M|^2$ of the decay. In ref. [21] this function is parametrized for decays into 3 pions by a series expansion of the form

$$|M|^2 \propto 1 + g \cdot \frac{s_3 - s_0}{m_{\pi^+}^2} + h \cdot \left(\frac{s_3 - s_0}{m_{\pi^+}^2} \right)^2 + j \cdot \frac{s_2 - s_1}{m_{\pi^+}^2} + k \cdot \left(\frac{s_2 - s_1}{m_{\pi^+}^2} \right)^2 + \cdots \quad ,$$

17

Decay mode	g	h	k
$K^{\pm} \longrightarrow \pi^{\pm} + \pi^{\pm} + \pi^{\mp}$	-0.22	0.01	-0.01
$K^{\pm} \longrightarrow \pi^0 + \pi^0 + \pi^{\pm}$	0.59	0.035	0.0
$K_L^0 \longrightarrow \pi^+ + \pi^- + \pi^0$	0.67	0.08	0.01
$K_L^0 \longrightarrow 3\pi^0$	0.0	0.0	0.0

Table 5.2: Coefficients of the parametrization of $K \longrightarrow 3\pi$.

Decay mode	λ_+	λ_0
$K^{\pm} \longrightarrow \pi^0 + e^{\pm} + \nu_e$	0.028	0.0
$K^{\pm} \longrightarrow \pi^0 + \mu^{\pm} + \nu_\mu$	0.033	0.004
$K_L^0 \longrightarrow \pi^{\pm} + e^{\mp} + \nu_e$	0.03	0.0
$K_L^0 \longrightarrow \pi^{\pm} + \mu^{\mp} + \nu_\mu$	0.034	0.025

Table 5.3: Coefficients of the parametrization of $K \longrightarrow \pi + \ell + \nu$.

where

$$s_i = (p_K - p_i)^2 = (m_K - m_i)^2 - 2 \cdot m_K \cdot E_i \qquad i = 1, 2, 3$$

$$s_0 = \frac{1}{3} \sum_i s_i = \frac{1}{3} \cdot (m_K^2 + m_1^2 + m_2^2 + m_3^2) \quad .$$

If CP invariance holds, j must be zero in good agreement with measurements. The values of the other coefficients are given in table 5.2.

The leptonic kaon decays show a probability density function that can be parametrized as described in ref. [22]

$$|M|^2 \propto G_+^2 \cdot \left[m_K \cdot (2 \cdot E_{\ell\,cm} \cdot E_{\nu\,cm} - m_K \cdot E'_\pi) + m_\ell^2 \cdot \left(\frac{1}{4} \cdot E'_\pi - E_{\nu\,cm} \right) + \right.$$
$$\left. H \cdot m_\ell^2 \cdot \left(E_{\nu\,cm} - \frac{1}{2} \cdot E'_\pi \right) + H^2 \cdot \frac{1}{4} \cdot m_\ell^2 \cdot E'_\pi \right]$$

with m_ℓ being the mass of the lepton and

$$H = \frac{m_K^2 - m_\pi^2}{m_\pi^2} \cdot (\lambda_0 - \lambda_+) \cdot G_-$$

$$G_{\pm} = 1 \pm \lambda_+ \cdot \frac{m_K^2 + m_\pi^2 - 2 \cdot m_K \cdot E_{\pi\,cm}}{m_\pi^2}$$

$$E'_\pi = \frac{m_K^2 + m_\pi^2 - m_\ell^2}{2 \cdot m_K} - E_{\pi\,cm} \quad .$$

The parameters λ_+ and λ_0 that fit the data best are given in table 5.3.

The energies are taken at random from these distributions. The cm angles θ and ϕ of the first secondary particle are chosen at random uniformly in the full

solid angle. The angle ψ of the reaction plane around the first particle direction is also chosen at random. As final step, the particle's kinematical parameters are transformed to the laboratory system.

5.5   Hyperon and η decays

The hyperons Λ and Σ are generated according to their production cross sections. Their average contribution to the charged and neutral multiplicity by their decay products (nucleons, pions, ...) is taken into account. In a similar way, the contributions of η mesons to the neutral multiplicity is included. In the present version of the program, the resonances Δ, K^*, and ρ are not explicitly accounted for.
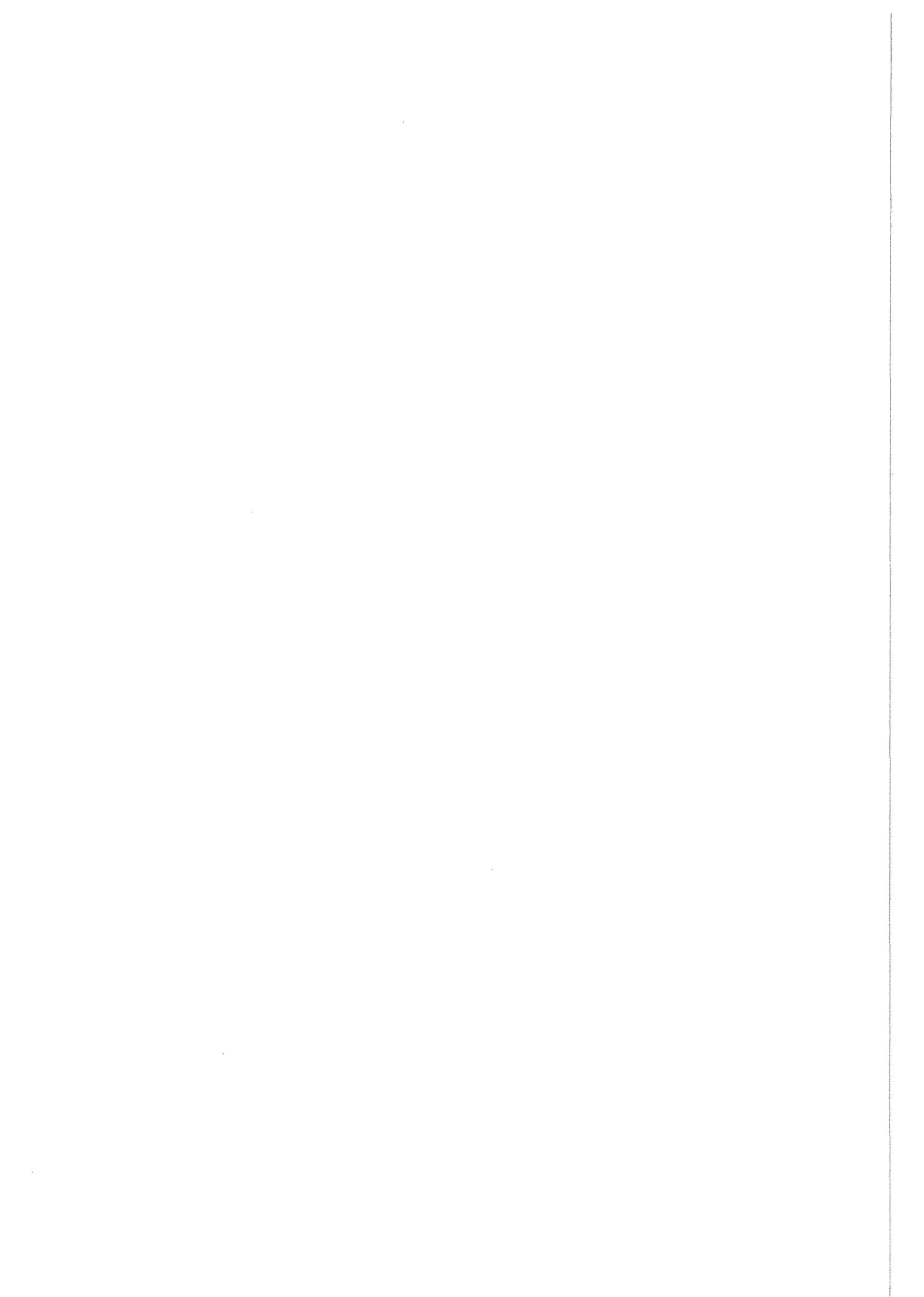
Chapter 6

Particle interactions

Hadronic interactions are described by two differnet models depending on energy If E_{cm} is above 10 GeV, the interaction is treated with a program based on the DPM. It is described in detail in section 6.1. Below this energy value, a simple isobar model is used for the particle interactions as explained in section 6.2. Electron and photon reactions are treated with EGS4 or with the analytic NKG formula (see section 6.3).

6.1   Strong interactions at high energies

As model of the interactions between hadrons and nuclei at high energies, an approach inspired by the DPM [4] and worked out by J.N. Capdevielle [3] was chosen. It is a phenomenological description of the interaction based on the picture that two dominant colour strings are formed between the interacting quarks of two hadrons. For instance, in a nucleon–nucleon collision, two chains (colour strings) are stretched between the fast valence di–quark of the projectile and one valence quark of the target and vice versa between the slow valence quark of the projectile and the di–quark of the target [4, 14]. The strings separate and fragment into many colour neutral secondaries that are produced around the primary quarks' directions. Such particle jets have been observed in many high energy physics experiments.

Recent experiments at $p\bar{p}$ colliders have improved the understanding of such reactions up to cm energies of 1.8 TeV. Unfortunately, the collider data contain mainly particles that are produced under large angles with respect to the direction of incidence (central rapidity region). But the major part of the energy escapes with the spectators in the beam pipe. For the development of EAS, however, the particles emitted in forward direction are the most important ones, because they carry the energy down through the atmosphere.

In the central region, many quantities, such as the number and type of secondaries, the longitudinal and transverse momentum distributions and the spatial energy flow have been measured and correlated with each other and with the available energy. The rich data collection of collider experiments has been used to build an interaction model that reproduces the collider results as well as possible.

A difficulty arises, because air shower simulations need a description of nucleon–nucleus or even nucleus–nucleus collisions rather than nucleon–nucleon interactions. In the following sections, it is described how these interactions are modelled on the basis of the present knowledge about nucleon–nucleon reactions.

6.1.1 Nucleon–nucleon interactions

Number of secondaries

The average charged–particle multiplicity (including the colliding particles) in nucleon–nucleon collisions has been measured up to cm energies of 1.8 TeV. It can be parametrized [23] as a function of $s = E_{cm}^2$ by

$$\langle n_{ch} \rangle = \begin{cases} 0.57 + 0.584 \cdot \log s + 0.127 \cdot \log^2 s & : & E_{cm} \leq 187.5\ GeV \\ 6.89 \cdot s^{0.131} - 6.55 & : & 187.5\ GeV < E_{cm} \leq 945.5\ GeV \\ 3.4 \cdot s^{0.17} & : & 945.5\ GeV < E_{cm} \end{cases} \quad . \tag{6.1}$$

The average number of neutral particles $\langle n_{neu} \rangle$ produced should be around $\langle n_{ch} \rangle/2$, the average total multiplicity around $\langle \mathcal{N} \rangle = 1.5 \langle n_{ch} \rangle$ at low energies. At high energies, however, a larger fraction of photons than expected by $n_\gamma = 2 \cdot n_{neu} = n_{ch}$, has been observed, mainly due to η meson production with subsequent decay into photons.

The average number of gamma quanta $\langle n_\gamma \rangle$ adopted to reproduce this excess follows the parametrization [24]

$$\langle n_\gamma \rangle = \begin{cases} -1.27 + 0.52 \cdot \log s + 0.148 \cdot \log^2 s & : & E_{cm} \leq 103\ GeV \\ -18.7 + 11.55 \cdot s^{0.1195} & : & E_{cm} > 103\ GeV \end{cases} \tag{6.2}$$

where $\langle n_\gamma \rangle$ is the average over many collisions, i.e. over all inclusive data. In contrast to $\langle n_\gamma \rangle$, we distinguish $\bar{n}_\gamma$ as the average number of photons in collisions with the same number of charged secondaries n_{ch}. The value of $\bar{n}_\gamma$ is deduced from the correlation

$$\bar{n}_\gamma = 2 + a \cdot n_{ch} \quad \text{with} \quad a = \begin{cases} 0.0456 \cdot \log s + 0.464 & : & E_{cm} < 957\ GeV \\ 1.09 & : & E_{cm} \geq 957\ GeV \end{cases}$$

We prefer this energy dependence of a compared to the constant value $a = 1.03$ given by the UA5 Collaboration [25], because it better describes the variations observed in the energy range $200\ GeV \leq E_{cm} \leq 900\ GeV$. For low energies, in any case, $\langle n_{neu} \rangle$ is forced to be at least equal to $\langle n_{ch} \rangle/2$.

The actual charged–particle multiplicity n_{ch} for each event fluctuates around the average value $\langle n_{ch} \rangle$. The fluctuations follow a negative binomial distribution

$$P(n_{ch}, \langle n_{ch} \rangle, k) = \binom{n_{ch} + k - 1}{n_{ch}} \cdot \left(\frac{\langle n_{ch} \rangle/k}{1 + \langle n_{ch} \rangle/k} \right)^{n_{ch}} \cdot \left(\frac{1}{1 + \langle n_{ch} \rangle/k} \right)^{k}$$

where P gives the probability to obtain n_{ch} particles for the parameters $\langle n_{ch} \rangle$ and k. The dependence of k on the cm energy E_{cm} is parametrized [26] by

$$1/k = -0.104 + 0.058 \cdot \log E_{cm} \quad .$$

From this distribution the actual number of charged particles n_{ch} is picked at random.

The actual number n_γ for a given collision is derived [27] from the observed relation between n_{ch} and n_γ in collider data [28]. For energies $E_{cm} > 200 \ GeV$, the probability distribution of n_γ around $\overline{n}_\gamma$ is described by a truncated Gaussian distribution, whose mean m and variance σ depend on $z = n_{ch}/\langle n_{ch} \rangle$ which is used as a convenient scaling variable.

$$m = \overline{n}_\gamma \cdot (0.982 - 0.376 \cdot e^{-z}) \cdot 0.92$$
$$\sigma = m \cdot (0.147 + 2.532 \cdot e^{-z}) \cdot 0.92 \quad .$$

At cm energies between 60 GeV and 200 GeV, the relation is given by

$$n_\gamma = n_{ch} \cdot (0.079 \cdot \log s - 0.001) + 0.391 \cdot \log s + 0.305$$

and below 60 GeV the fluctuations are taken to be the same as for the charged particles $n_\gamma = z \cdot \langle n_\gamma \rangle$.

The parent particles of the photons are assumed to be mainly neutral pions, but also ρ and η mesons, kaons, and hyperons can contribute to the γ component.

Particle ratios

The abundances of kaons, nucleons, Λ and Σ particles in nucleon–nucleon collisions were measured by the UA5 collaboration. We adopt the UA5 parametrization [25] of the ratio of charged kaon to charged pion numbers

$$n_{K^\pm}/n_{\pi^\pm} = 0.024 + 0.0062 \cdot \log s \qquad (6.3)$$

and the ratio of the number of nucleons to the number of all charged particles

$$n_N/n_{ch} = -0.008 + 0.00865 \cdot \log s \quad . \qquad (6.4)$$

Λ, Σ^0, and $\Sigma^\pm$ particles are produced with the same probability and their ratio to the number of all charged particles is

$$\frac{n_\Lambda}{n_{ch}} = \frac{n_{\Sigma^0}}{n_{ch}} = \frac{n_{\Sigma^+} + n_{\Sigma^-}}{n_{ch}} = \frac{1}{2}(0.0238 + 0.00978 \cdot \log s)^2$$

as derived from hyperon production data [29]. A noticeable contribution to photon production originates from η mesons. Their abundance relative to all charged particles is derived from [30]

$$n_\eta/n_{ch} = 0.0162 \cdot \log s - 0.0177 \quad .$$

Taking into account all these particle ratios and the specific decay modes of the particular particles, all the particle numbers of nucleons, pions, kaons, etas, and hyperons are determined to meet the previously selected charged and neutral multiplicity n_{ch} and n_γ for each single collision.

Rapidity distribution

In hadronic reactions jets of secondary particles are generated by the hadronizing colour strings. The kinematics of particles of a jet are described by their transverse momenta p_T and rapidities y where the latter are defined by

$$y = \frac{1}{2} \cdot \log \frac{E + p_L}{E - p_L}$$

with E being the particle energy and p_L the longitudinal momentum. In the representation of rapidity and transverse momentum, the rapidities of the particles of a jet are approximated by a Gaussian distribution as suggested by Klar and Hüfner [47] and by inelastic hadron–hadron and lepton–hadron scattering data [31, 32]. The two principal jets of a collision are back–to–back in the center of mass and therefore positioned symmetrically around $y_{cm} = 0$ in rapidity space. The average positions of the centers of the respective Gaussians on the rapidity axis in the cm system $\langle y_{mean} \rangle$ and the average width $\langle \sigma_y \rangle$ are parametrized based on experimental data for nucleon–nucleon collisions [3].

$$
\begin{aligned}
\langle y_{mean} \rangle &= \pm(0.146 \cdot \log(s - 1.76) + 0.072) \\
\langle \sigma_y \rangle &= 0.12 \cdot \log(s - 1.76) + 0.18 \quad .
\end{aligned}
\tag{6.5}
$$

The rapidity of the cm system in the laboratory frame is expressed by

$$y_{cm} = \frac{1}{2} \cdot \log \frac{E_{lab} + m_N + p_{lab}}{E_{lab} + m_N - p_{lab}}$$

with m_N being the nucleon mass and p_{lab} the nucleon momentum in the laboratory system. The amplitude of the rapidity distributions is determined by deducing the central rapidity density from data. Experimentally, however, only the pseudorapidity

$$\eta = -\log \tan \frac{\theta}{2}$$

with θ being the cm production angle, is directly observed. The average pseudorapidity density in the central region

$$\langle \rho_{\eta=0} \rangle = \langle \frac{dN}{d\eta}_{\eta=0} \rangle$$

as a function of the cm energy is obtained from non single diffractive data [23] as

$$
\langle \rho_{\eta=0} \rangle = \begin{cases} 0.82 \cdot E_{cm}^{0.214} & : \quad E_{cm} \leq 680 \; GeV \\ 0.64 \cdot E_{cm}^{0.252} & : \quad E_{cm} > 680 \; GeV \quad . \end{cases}
\tag{6.6}
$$

The conversion from the measured mean pseudorapidity density in the central region to the needed central rapidity density $\rho_{y=0} = \frac{dN}{dy}_{y=0}$ is performed depending on the scaling variable z [3]

$$
\rho_{y=0} = \begin{cases} \langle \rho_{\eta=0} \rangle \cdot f_{\eta \to y} \cdot (0.487 \cdot z + 0.557)^2 & : \quad z \geq 1.5 \\ \langle \rho_{\eta=0} \rangle \cdot f_{\eta \to y} \cdot (0.702 \cdot z + 0.244)^2 & : \quad z < 1.5 \end{cases}
\tag{6.7}
$$

24

with the conversion factor from pseudorapidity to rapidity

$$f_{\eta \to y} = \langle \rho_{y=0} \rangle / \langle \rho_{\eta=0} \rangle = 1.25$$

kept constant.

Recent calculations with the DPM [14] suggest a more accurate parametrization for both $\langle \rho_{\eta=0} \rangle$ and $\langle \rho_{y=0} \rangle$ up to $\sqrt{s} = 5 \cdot 10^4 \ GeV$ which is

$$\begin{aligned}
\langle \rho_{\eta=0} \rangle &= 0.264 \cdot \log s - 0.216 \\
\langle \rho_{y=0} \rangle &= 0.313 \cdot \log s + 0.063 \quad .
\end{aligned} \qquad (6.8)$$

Following these parametrizations $f_{\eta \to y}$ becomes energy dependent and replaces the constant factor 1.25 in the eqs. 6.7. The differences between this and the previous parametrizations (eqs. 6.6 and 6.7) are small in the energy range accessible by the experiments. Nevertheless the new description (eqs. 6.8) provides a more consistent basis for the extrapolation to higher energies.

The amplitude A_y of the Gaussians is deduced from the requirement that all particles belong to the Gaussians

$$\int_{-\infty}^{+\infty} \frac{dN}{dy} dy = n_{ch} \qquad \text{leading to} \qquad A_y = n_{ch}/(\sigma_y \cdot 2\sqrt{2\pi}) \quad .$$

The position of the Gaussians on the rapidity axis is now calculated such that the central rapidity density seen in semi–inclusive data is obtained by adding the two rapidity distributions in the center

$$\rho_{y=0} = 2 \cdot A_y \cdot e^{-y_{mean}^2/2\sigma_y^2} \quad .$$

Thus, y_{mean} is computed by

$$y_{mean} = \sigma_y \cdot \sqrt{2 \cdot \log(2 \cdot A_y/\rho_{y=0})} \quad .$$

The quantity σ_y is taken to be $\langle \sigma_y \rangle$. The advantage of this procedure is to find immediately the natural position of the set of rapidities.

In case of parent particles of photons, the same procedure as for charged particles is applied to fix the position of the Gaussians as required to reproduce the theoretical central rapidity densities. Optionally a slightly modified procedure may be adopted to achieve a better agreement with experimental results [24, 33] which suggest a narrower rapidity distribution for photons. The central rapidity densities $\rho_{y=0}^\gamma$ are determined from eqs. 6.7 by replacing the scaling variable z by $z_\gamma = n_\gamma/\langle n_\gamma \rangle$ and multiplying it with 0.5 to account for the average ratio of neutral to charged pions and with an energy dependent factor $g(E_{cm})$ given by

$$g(E_{cm}) = \begin{cases} 1 & : \quad E_{cm} \leq 50 \ GeV \\ 1 + 0.18 \cdot \log(E_{cm}/50 \ GeV) & : \quad 50 \ GeV < E_{cm} \leq 200 \ GeV \\ 1.25 & : \quad 200 \ GeV < E_{cm} \end{cases}$$

25

As in case of charged particles, the calculations of Attallah et al. [34] suggest a more refined treatment of the conversion factor from pseudorapidity to rapidity also for the neutrals

$$f^\gamma_{\eta \to y} = \frac{\langle \rho^\gamma_{y=0} \rangle}{\langle \rho^\gamma_{\eta=0} \rangle} = \begin{cases} 1.1 & : & E_{cm} \leq 19.4 \; GeV \\ 1.33 - 0.0391 \cdot \log(s - 1.76) & : & 19.4 \; GeV < E_{cm} \leq 900 \; GeV \\ 0.8 & : & 900 \; GeV < E_{cm} \end{cases}$$

to take into account UA5 results [24].

For each particle its rapidity y_i in the cm system is chosen from the appropriate Gaussian distribution at random.

Transverse momentum of the secondaries

The transverse momentum distribution of secondaries in nucleon–nucleon collisions is well described [35] by

$$\frac{d^2 N}{dp_x dp_y} \propto \left(\frac{p_0}{p_0 + p_T} \right)^n \quad .$$

With $p_T = \sqrt{p_x^2 + p_y^2}$ one obtains the probability density function

$$\frac{dN}{dp_T} = \frac{(n-1) \cdot (n-2)}{p_0^2} \cdot \left(\frac{p_0}{p_0 + p_T} \right)^n \cdot p_T \tag{6.9}$$

where $p_0 = 1.3 \; GeV/c$ for pions and the parameter n depends on the central pseudorapidity density $\rho_{|\eta|<D}$ as [36]

$$n = 7.4 + 3.67/\rho_{|\eta|<D}^{0.435}$$

The density $\rho_{|\eta|<D}$ is calculated from the central region of width $2D$ with $D = 0.67 \cdot (2.95 + 0.03 \cdot \log s)$. According to this distribution, the transverse momenta are determined for secondary pions only. As there is experimental evidence [37] on differences between the transverse momentum distributions of secondary pions, kaons and nucleons, this is accounted for by applying energy dependent correction factors $\langle p_T^K \rangle / \langle p_T^\pi \rangle$ and $\langle p_T^N \rangle / \langle p_T^\pi \rangle$ with

$$\langle p_T^\pi \rangle(s) = \begin{cases} 0.3 + 0.00627 \cdot \log s & : & E_{cm} < 132 \; GeV \\ (0.442 + 0.0163 \cdot \log s)^2 & : & E_{cm} \geq 132 \; GeV \end{cases}$$

$$\langle p_T^K \rangle(s) = \begin{cases} 0.381 + 0.00797 \cdot \log s & : & E_{cm} < 131 \; GeV \\ (0.403 + 0.0281 \cdot \log s)^2 & : & E_{cm} \geq 131 \; GeV \end{cases}$$

$$\langle p_T^N \rangle(s) = \begin{cases} 0.417 + 0.00872 \cdot \log s & : & E_{cm} < 102 \; GeV \\ (0.390 + 0.0341 \cdot \log s)^2 & : & E_{cm} \geq 102 \; GeV \end{cases} \quad .$$

A slight inconsistency should be noted. Instead of using the energy dependence of $\langle p_T^\pi \rangle$ from eq. 6.9 the $\log s$ parametrization is used in the correction factors only.

The advantage of this method is to follow closely the correlation of $\langle p_T \rangle$ with the average central rapidity density.

The sum $S_{p_T} = \sum_i^N p_{T,i}$ of the transverse momenta of all secondaries is calculated and the p_T values of the particles are reduced by S_{p_T}/N to fulfill transverse momentum conservation.

Energy of the secondaries

The laboratory energy of particle i is calculated according to

$$E_i = \sqrt{p_{T,i}^2 + m_i^2} \cdot \cosh(y_i + y_{cm})$$

for all but one particle. This 'last' particle gets the remaining energy to fulfill energy conservation. In case this is not possible, because there is not enough energy left, the particle generation is repeated. The sum of the secondary particles' energies (except the last particle) determines the inelasticity of the reaction. It is not an adjustable parameter but emerges from the interaction model.

Treatment of leading particles and charge exchange

In high energy collisions, about 50% of the cm energy is carried away by secondary particles, which is usually noted as an inelasticity parameter $k \approx 0.5$. This value is reproduced rather well by the CORSIKA generator without any additional constraint. By attributing the remaining energy to the last particle, this will in general be the most energetic one. It is called the leading particle.

Two further alternatives have been proposed in literature to determine the leading particle's rapidity. Alner et al. [25] attribute the largest of the randomly selected rapidities of the secondaries to the leading particle. The second alternative picks the leading particle's rapidity from a separate distribution resulting from DPM calculations [38] for the valence quarks recombined in the final state. There is no decisive argument yet in favor of one of the three treatments, hence, the additional alternatives will be added as options in a future version.

The leading particle after the collision is correlated with the primary incoming particle due to the fact that the fast spectator quarks of the interaction move almost with their initial velocity and most likely form the fastest secondary particle together with a sea quark. This picture limits the possible types of leading particle that can appear for a given primary. Besides the cases where the leading particle is of the same type as the incoming one, a charge exchange reaction may occur. The processes which are taken into account are listed in table 6.1. The probability for charge exchange varies with energy as

$$P_{ex} = 2 - 2 \cdot e^q \quad \text{with} \quad q = \begin{cases} -2.055 \; GeV/E_{cm} - 0.0913 & : \quad E_{cm} \leq 40 \; GeV \\ -5.7 \; GeV/E_{cm} & : \quad E_{cm} > 40 \; GeV \end{cases}$$

giving $P_{ex} \approx 0.5$ at $E_{cm} = 10 \; GeV$ which is the low end of the DPM energy regime and dropping to 0.01 at $E_{cm} = 1000 \; GeV$ ($E_{lab} \approx 5 \cdot 10^{14} \; eV$). The charge exchange reactions may be suppressed by a control flag.

fast		slow		fast		slow
p	+	n	$\longrightarrow$	n	+	p
n	+	p	$\longrightarrow$	p	+	n
π^-	+	p	$\longrightarrow$	π^0	+	n
π^+	+	n	$\longrightarrow$	π^0	+	p
π^0	+	p	$\longrightarrow$	π^+	+	n
π^0	+	n	$\longrightarrow$	π^-	+	p
K^-	+	p	$\longrightarrow$	$K^0_{L/S}$	+	n
K^+	+	n	$\longrightarrow$	$K^0_{L/S}$	+	p
$K^0_{L/S}$	+	p	$\longrightarrow$	K^+	+	n
$K^0_{L/S}$	+	n	$\longrightarrow$	K^-	+	p

Table 6.1: Charge exchange reactions of the leading particle.

The leading particle in a high energy collision may also be a Δ^-, Δ^0, Δ^+, or Δ^{++} resonance in case of nucleon induced collisions, a vector meson $\rho^\pm$ or ρ^0 for pion induced ones, or a strange vector meson K^* for primary kaons with important consequences for the hadron cascading in EAS [39] due to subsequent decay or modified penetration depth in case of decay to the electromagnetic channel. The transverse momentum of the leading particles should be modified in order to respect the change of the p_T distribution with increasing Feynman x (seagull effect). The correction may be introduced following NA27 results [33]. This has not yet been done but will be considered in a following program version.

Diffractive processes

Most of the particles do not experience completely central collisions. In peripheral collisions it may happen that the projectile is just excited by a rather small energy and momentum transfer from a target nucleon. The excited projectile subsequently decays and forms secondary particles. Such interactions are called diffractive processes. Their topology is different from the non–diffractive events, mainly due to the reduced amount of energy E_{SD} that is available for production of secondary particles. As suggested by experimental data [40], a fraction of 15% of all interactions is assumed to be diffractive in the present version of the program. Strictly speaking, the ratio of diffractive to total cross section is slightly energy dependent following the parametrization by [14]

$$\sigma_{SD} = \left(1.77 \cdot \log^{0.7} s - 2.38 \right) mb \quad .$$

In principle, diffractive interactions are treated in the same way as non–diffractive processes, with the following differences. First, experimental results [41] and theo-

retical predictions [42] indicate the excitation energy E_{SD} to follow

$$\frac{d\sigma_{SD}}{d(E_{SD}^2/s)} \propto \frac{1}{E_{SD}^2/s} \quad .$$

E_{SD} must be large enough to produce at least one additional pion, but is limited to at maximum 5% of the cm energy.

Second, the position and width of the Gaussians in rapidity space are calculated as indicated in eq. 6.5, however, replacing s by $s_{SD} = E_{SD}^2$. With the same substitution the excess of photons from decaying secondaries is described as explained in eq. 6.2, and the particle ratios of kaons and nucleons to pions are calculated following eqs. 6.3 and 6.4.

Third, hyperon production in diffractive interactions is neglected.

Following the data, however, a modified parametrization of the average central pseudorapidity density [43]

$$\langle \rho_{\eta=0} \rangle = 0.74 \cdot E_{SD}^{0.21} + 0.2325$$

is introduced. The average number of charged particles varies with the energy in the same way as for the non–diffractive case [44, 45]. Therefore, we adopt the parametrization of eqs. 6.1 and replace s by s_{SD}.

With these parametrizations the same procedure is followed to generate secondaries, their energies and transverse momenta, and to conserve the energy and momentum as in the non–diffractive case. Due to the smaller amount of energy available the overall number of secondaries is smaller. This leads to a larger fraction of rejections due to energy mismatch.

6.1.2 Nucleon–nucleus interactions

In an EAS the incoming particle does not collide with free nucleons but with nuclei of the air target. Consequently, the interaction model has to be adapted to this situation. Since the nucleon–nucleon interactions are experimentally well studied, we try to construct the nucleon–nucleus interaction basically in terms of the nucleon–nucleon interaction.

The treatment of nucleon–nucleus or nucleus–nucleus interactions starts with the identification of the type of target nucleus. Therefore, the relative contributions of the various air nuclei to the total inelastic cross section have been calculated and the choice is made at random according to these contributions.

When a high energy nucleon hits an air nucleus, it does not interact with the whole nucleus, but with a few target nucleons only. The number n_T of ('wounded') target nucleons hit by the projectile can be determined in two different manners. Either, a parametrization of $\langle n_T \rangle$ depending on the target mass number A_{target} and the square of the cm energy s is used [3]

$$\langle n_T \rangle = (0.56 + 0.0236 \cdot \log(s - 1.76)) \cdot A_{target}^{0.31} \tag{6.10}$$

29

neglecting the fluctuations of n_T around its mean value. In the second option n_T is explicitly selected according to its probability distribution [46] which is obtained by Glauber calculations.

In case of diffractive interactions, we either set $n_T = 1$ or calculate it according to eq. 6.10 with s being replaced by s_{SD}.

Thus, the primary particle is assumed to interact with n_T nucleons of the target successively. Obviously the multiple interactions in one nucleus are not independent of each other. Our approach accounts for the multiple interactions in the target by several corrections based on an analysis by Klar and Hüfner [47]. The main one is the production of additional secondaries, the target excess. This excess was measured by observing the extra negative particles Δn_- from nucleon–nucleus collisions and was parametrized [47] as

$$\langle \Delta n_- \rangle = \begin{cases} 0.285 \cdot (n_T - 1) \cdot \langle n_{ch} \rangle & : \quad E_{cm} \leq 137 \; GeV \\ 0.25 \cdot (n_T - 1) \cdot \langle n_{ch} \rangle & : \quad E_{cm} > 137 \; GeV \end{cases} .$$

The neutral excess is then $\langle \Delta n_{neu} \rangle = \langle \Delta n_- \rangle$ and the number of additional charged particles from the target excess is $\langle \Delta n_{ch} \rangle = 2 \langle \Delta n_- \rangle$. The additional particles originate from a third string which is modelled by a third Gaussian distribution in rapidity space.

When choosing the energies of the particles from the target excess, the rapidities are taken at random from the third Gaussian. The particle types of the target excess are determined following the same ratios as are used for the other secondaries.

The parametrization of position y_m and width σ of this Gaussian, depending on the number of reacting target nucleons n_T, is given [3] by

$$y_m = -3 + 2.575 \cdot e^{-0.082 \cdot n_T}$$
$$\sigma = 1.23 + 0.079 \cdot \log n_T \quad .$$

The final position of the third Gaussian is chosen in full analogy with the procedure described above such that the particle excess in the center of rapidity equals the observed values $\rho_{y=0}^{SD}$ with [48]

$$\rho_{y=0}^{SD} = \rho_{y=0} \cdot \frac{n_T - 1}{2} \quad .$$

The target excess lies at negative rapidity values in all cases.

According to HELIOS results [49] we assume the ratio of diffractive to total inelastic cross section to be the same for nucleon–nucleon and nucleon–nucleus collisions.

6.1.3 Pion–nucleon and kaon–nucleon interactions

The interactions of pions and kaons with a nucleus are simulated in strict analogy with the nucleon–nucleus interaction. Only for the calculation of the available cm

energy and the determination of the number of target nucleons involved in the interaction process, the different masses and cross sections of pions and kaons are taken into account. All other features described in the nucleon case are the same for pions and kaons.

6.1.4 Nucleus–nucleus interactions

As described in section 3.2.2, the probabilities of n_P projectile nucleons interacting and the probability of a projectile nucleon to interact with n_T target nucleons were also calculated by the Glauber theory [15, 46]. Following these probabilities, the number of interacting projectile nucleons n_P is selected at random. The further reaction is now regarded as a superposition of n_P nucleon–nucleus reactions which are simulated as described in section 6.1.2. The ratio of interacting protons and neutrons is assumed to be equal to the ratio in the parent nucleus.

For the non–interacting nucleons of the projectile, the so called spectators, two options exist [50]. First, they can be regarded as free nucleons with their initial velocity. They are stored on the internal particle stack and are processed further at a later time. This option assumes the complete fragmentation of the projectile nucleus in the first interaction. The second option of fragmentation keeps all spectators together as one nucleus propagating further through the atmosphere and reacting later on. These two options, being the limiting cases of what really happens in nature, allow to estimate the influence of the fragmentation on the results of the air shower simulations. Our calculations show that the differences between the two cases are small and details of nuclear fragmentation are smeared out by fluctuations.

6.2 Strong interactions at low energies

The DPM reaches its limits when the cm energy available for generation of secondary particles drops below a certain value. This value is presently set at 10 GeV. In an EAS, however, the bulk of particles interact at cm energies far below that value.

Therefore, the isobar model of P.K.F. Grieder [2] was adopted to simulate hadronic reactions at cm energies between 0.3 GeV and 10 GeV. In this model the hadron–nucleus collisions are approximated by hadron–nucleon reactions. The non interacting nucleons of the target are neglected. The hadron–nucleon reactions are assumed to take place via several intermediate states which are decaying immediately in up to 5 secondaries. The intermediate state can be a single particle, a heavy non–strange or strange meson, or a light or a heavy isobar. Intermediate states produced simultaneously share the available cm energy according to their masses and move only forward or backward with respect to the laboratory direction. The single particle can be a nucleon, pion, or kaon going forward and a recoil nucleon going backward in the cm system. The heavy and strange mesons have a mass of $m_{HM} = m_{SM} = 1.35 \ GeV/c^2$ and decay into three pions or two pions and a kaon, respectively. The light isobar of mass $m_{LI} = 1.4 \ GeV/c^2$ fragments into one

pion and a nucleon, whereas the heavy isobar with mass $m_{HI} = 2.5\ GeV/c^2$ decays into one nucleon and three or four pions.

These intermediate states cannot be identified with single well established particles or resonances, but are to represent the manifold of short lived states observed in this energy region which decay mostly into few secondaries.

6.2.1 Processes of hadronic reactions

Which of the intermediate states are produced depends on the parent particle and its energy. A nucleon, for instance, produces two heavy isobars, if the available cm energy is $5.5\ GeV < E_{cm} \le 10\ GeV$, a heavy isobar and a single nucleon for $3.5\ GeV < E_{cm} \le 5.5\ GeV$, and a light isobar and a single nucleon for $2.5\ GeV < E_{cm} \le 3.5\ GeV$. The isobars can go forward or backward in the laboratory system. Below $E_{cm} = 2.5\ GeV$, only elastic scattering can occur. The elastic scattering changes the particle's direction but not its energy. In addition to these processes antinucleons may annihilate.

For pion reactions in the energy range of $3.9\ GeV < E_{cm} \le 10\ GeV$ a heavy isobar and a heavy meson are produced. For $2.7\ GeV < E_{cm} \le 3.9\ GeV$ a heavy isobar and a single pion or a heavy meson and a single nucleon can appear in competition. A light isobar and a single pion are the products of a reaction at $1.6\ GeV < E_{cm} \le 2.7\ GeV$ and below $E_{cm} = 1.6\ GeV$ only elastic scattering is possible. As the incoming pion tends to be emitted in forward direction, the heavy meson and the single pions are always produced in forward direction in the cm system.

In the energy range of $3.9\ GeV < E_{cm} \le 10\ GeV$ kaons produce a heavy isobar and a strange meson. For $3.05\ GeV < E_{cm} \le 3.9\ GeV$ a heavy isobar and a single kaon or a strange meson and a single nucleon may appear alternatively. A light isobar and a single kaon are produced at $1.6\ GeV < E_{cm} \le 3.05\ GeV$ and below again only elastic scattering occurs. The reaction products are ordered in such a way that the kaon or strange meson always emerge into forward direction, i.e. following the direction of the incoming kaon.

Isobars

The isobars decay immediately into one nucleon and one or more pions depending on the isobar's mass. The pion charges are selected at random considering charge conservation.

If the isobar is going forward in the cm system, the transverse and longitudinal momenta p_T, p_L of the pions are picked from the probability distributions

$$P(p_T) = \frac{p_T}{0.1 GeV} \cdot e^{-p_T/0.1 GeV} \tag{6.11}$$

$$P(p_L) = \frac{1}{0.1} \cdot e^{-p_L/0.1 GeV} \tag{6.12}$$

32

where the peak value of the transverse momentum distribution and the mean value of the longitudinal momentum distibution are both fixed to 0.1 GeV.

It is decided at random, whether the pions move forward or backward in the cm system and which charge they carry. The transverse momentum of the nucleon is finally selected at random as in the case of pions, whereas its longitudinal momentum is chosen in a way that energy is conserved. The sign of p_L is chosen to minimize the sum of p_L over all particles. For nucleons charge exchange is possible.

If the isobar is emitted backward in the cm system, the procedure is different. The isobar is assumed to be a recoil particle and the energy of all its decay products (nucleon and pions) is picked from a uniform energy spectrum ranging up to half of the isobar's rest energy. The transverse momenta are picked according to eq. 6.11.

Heavy and strange mesons

The procedure to produce secondary pions or kaons from heavy and strange meson decays resembles that for isobars. The secondaries' charges are chosen at random. The momenta p_T and p_L are selected according to eqs. 6.11 and 6.12, the sign of p_L in the cm system is determined at random. The last particle gets a random p_T, but p_L is chosen to conserve the energy and to minimize Σp_L.

Single particle

The energy E_{SP} and direction of the single hadron is in principle determined by E_{cm} and the masses of the hadron and the accompanying intermediate state. However, deviations from this direction of the order of a typical p_T as given by eq. 6.11 are allowed. The single nucleons and pions obtain their charge by random selection, single kaons keep the identity of the incoming kaon. Recoil nucleons are protons or neutrons with equal probability, their energy is limited to $E_{SP}/2$ and distributed uniformly and their transverse momentum is taken from eq. 6.11.

Annihilation of antinucleons

As antinucleons travel through the atmosphere they can undergo annihilation with a nucleon. The annihilation cross section is in the order of 10% of the inelastic cross section at a cm energy of 10 GeV strongly increasing with falling energies (see eq. 3.5). Various final states have been studied experimentally [51] and are listed in table 6.2 with their branching ratios.

The longitudinal and transverse momenta of the annihilation products have been measured for different final state multiplicities [52, 53]. In order to describe the experimental results, the p_T distribution of eq. 6.11 had to be modified by a correction factor F depending on the total multiplicity $\mathcal{N}$ and the cm energy E_{cm}

$$F(\mathcal{N}, E_{cm}) \propto \mathcal{N}^{-1.5} \cdot E_{cm} \quad .$$

The experimental longitudinal momentum distributions [53] show approximately Gaussian shapes. We therefore take the values of p_L at random from a Gaussian

$\bar{p}p$, $\bar{n}n$:		$\bar{p}n$, $\bar{n}p$:	
Decay mode	Branching ratio (%)	Decay mode	Branching ratio (%)
$\pi^+ \pi^-$	0.42	$\pi^+ \pi^0$	0.2
$\pi^+ \pi^- \pi^0$	7.28	$\pi^+ 3\pi^0$	8.0
$\pi^+ \pi^- 2\pi^0$	9.81	$\pi^+ 4\pi^0$	9.0
$\pi^+ \pi^- 3\pi^0$	24.58	$\pi^+ 5\pi^0$	0.7
$\pi^+ \pi^- 4\pi^0$	2.95	$2\pi^+ \pi^-$	6.54
$2\pi^+ 2\pi^-$	6.54	$2\pi^+ \pi^- \pi^0$	17.0
$2\pi^+ 2\pi^- \pi^0$	18.88	$2\pi^+ \pi^- 2\pi^0$	10.0
$2\pi^+ 2\pi^- 2\pi^0$	17.51	$2\pi^+ \pi^- 3\pi^0$	26.0
$2\pi^+ 2\pi^- 3\pi^0$	4.43	$2\pi^+ \pi^- 4\pi^0$	4.0
$3\pi^+ 3\pi^-$	2.11	$3\pi^+ 2\pi^-$	4.2
$3\pi^+ 3\pi^- \pi^0$	1.79	$3\pi^+ 2\pi^- \pi^0$	12.0
$3\pi^+ 3\pi^- 2\pi^0$	0.32	$3\pi^+ 2\pi^- 2\pi^0$	6.6
$4\pi^0$	3.38		

Table 6.2: Annihilation final states and branching ratios.

distribution with a mean value of

$$\langle p_L \rangle^2 = \frac{1}{\mathcal{N}} \left(E_{cm}^2 - \sum_{i=1}^{\mathcal{N}} (m_i^2 + p_{T\,i}^2) \right)$$

which shares the available energy after subtraction of the transverse mass among all the particles. Strict momentum conservation is obtained by correcting all momentum vectors by

$$\vec{p}_{i\ new} = \vec{p}_{i\ old} - S_{\vec{p}} \qquad i = 1, 2, \ldots \mathcal{N}$$

with

$$S_{\vec{p}} = \frac{1}{\mathcal{N}} \cdot \sum_{i=1}^{\mathcal{N}} \vec{p}_i \quad .$$

If the sum of the particle energies deviates from the cm energy by more than 1%, a second correction is applied with a factor deduced from the ratio $E_{cm} / \sum_{i=1}^{\mathcal{N}} E_i$. To conserve the transverse momentum distribution of eq. 6.11 as far as possible, the relative change of the transverse momenta is taken smaller by a factor of 20 than that of the longitudinal momenta. This correction is iterated until the energies match within 1%. The convergence of this procedure is accelerated by choosing a correction factor depending on the energy of the annihilating antinucleon and on the number of the secondary particles.

6.2.2 Charge, energy and momentum conservation

The recipes to attribute charge, energy and momentum to the secondary particles
are not very sophisticated. Charge, energy and momentum are not strictly conserved
for each reaction, but only on average over many processes. In the development of
an EAS the number of reacting particles and interactions becomes large enough to
ensure global energy and momentum conservation.

6.3 Electromagnetic interactions

6.3.1 Electron gamma shower program EGS4

The EGS4 option enables a full Monte Carlo simulation of the electromagnetic com-
ponent of showers by calling the EGS4 package which for electrons or positrons
treats annihilation, Bhabha scattering, bremsstrahlung, Møller scattering, and mul-
tiple scattering (according to Molière's theory). Gamma rays may undergo Compton
scattering, e^+e^- pair production, and photoelectric reaction. The programming of
these standard interactions is well documented in ref. [5] and therefore not described
here. The direct $\mu^+\mu^-$ pair production and the photonuclear reaction with protons
and neutrons of nuclei of the atmosphere have been added. Despite their small cross
sections, these two processes are essential for the muon production in gamma ray
induced showers.

Photoproduction of muons and hadrons

The $\mu^+\mu^-$ pair formation is treated in full analogy with the e^+e^- pair formation
replacing the electron rest mass by the muon rest mass.

The parametrization of the photonuclear reaction cross section [54] used com-
prises three resonances at 0.32 GeV, 0.72 GeV and 1.03 GeV superimposed on a
continuum which slightly increases with energy. Its value at 21 TeV is in excellent
agreement with the preliminary HERA data [55]. The cross sections and branching
ratios for all electromagnetic processes are provided in a cross section file as usual
in EGS4.

In photonuclear reactions the target nucleons are treated as free particles with the
assumption that only one nucleon is involved in the photonuclear process. Various
possibilities exist to generate secondary particles which are selected depending on
the energy of the gamma ray. Below 0.4 GeV only one pion is generated, while
in the subsequent range up to 1.4 GeV the chance to generate one pion decreases
linearly in favour of the generation of two pions. The choice between these two
possibilities is made at random. Between 1.4 GeV and 2 GeV always two pions are
produced. Within the range of 2 GeV < E_γ < 3 GeV the selection between two
pion generation and the DPM option is made at random with a linearly decreasing
chance for two pion generation. Above 3 GeV multi–particle production by the
DPM is always assumed.

During production of one single pion, the recoil nucleon may undergo charge exchange with 50% probability. The pion's azimuthal angle is chosen at random from a uniform distribution, while the polar angle is selected by a rejection method which produces a dipole or a quadrupole radiation characteristics depending on the energy of the gamma ray. If a charged pion is produced, these characteristics are modified to meet approximately the experimentally determined angular distributions [56].

When two pions together with a recoil nucleon are produced the particle energies are chosen to fall inside a Dalitz plot with a constant probability density. The treatment is analogous to the K decay into three secondary particles (see section 5.4). Charge exchange of the recoil nucleon is allowed giving altogether 6 exit channels which are given equal chance respecting charge conservation. The production of more than two secondary particles is treated by the DPM as described in section 6.1. In this case a neutral pion is assumed to be the leading particle and diffraction is suppressed.

Modifications of the standard EGS4

The essential modifications of the standard EGS4 code [5] are summarized as follows.

Particle identification, observation levels, and random number generator are adapted to the standards of CORSIKA.

The propagation time (including fast renormalization of direction cosines) is calculated for the total curved path length of the particles also in the case of magnetic field deflection.

The barometric density dependence of air as described in section 2.4 is implemented into the particle tracking used within the EGS4 routines. Important is the path length correction of the mean free path to the next interaction.

The deflection of electrons and positrons in the earth's magnetic field (see section 4.3) is calculated by an approximation only valid for small deflection angles [5]. As low energy particles at high altitude may have considerable path lengths and, hence, large deflection angles, the step size is limited to keep the deflection angle below $11.5°$ for each step.

The pressure dependence of the Sternheimer correction [57] for ionization losses in air is modified. The standard EGS4 cross section files contain the continuous energy loss dE/dx of electrons and positrons for energies above $1 MeV$ by ionization in gaseous matter depending on the pressure at a fixed density. The deposited energy per radiation length X_0 in air rises linearly with the logarithm of the energy in MeV as

$$dE/dx = (61.14 + 5.58 \cdot \log E) MeV/X_0$$

until it saturates at an energy that depends on the pressure. Expressed as a function of height h in cm, the saturation energy loss is

$$(dE/dx)_{sat} = (86.65 + 8 \cdot 10^{-6} \cdot h) MeV/X_0 \quad .$$

This approximates the pressure dependence of the energy loss by ionization to better than 5%.

The reduction of computing time becomes important with increasing primary energy, as this time increases linearly with the energy dissipated in the atmosphere. Therefore, the probability of electrons or gamma rays to produce a charged particle at the next observation level is estimated [58] as a function of their altitude and energy. If the probability remains below a preselected lower limit depending on shower size, this particle is discarded unless it is closer than 3 radiation lengths to the next observation level, the gamma ray energy exceeds the pion production threshold of 152 MeV, or the electron energy twice exceeds this threshold value. The latter conditions assure, that the production of pions which may decay into muons with large penetration depth is not suppressed. This discarding mechanism eliminates the numerous calculations of low–energy subshowers which do not contribute to observable particles and reduces the computation time by a factor of 3.

It should be emphasized that the thresholds for the discarding mechanism should be lowered appropriately, if production of Cerenkov radiation is incorporated into the program.

6.3.2 Nishimura–Kamata–Greisen formula

In the NKG option the electromagnetic component of air showers is calculated by an analytical approach [59] without a full Monte Carlo simulation. The advantage of very modest computer time requirements for the analytical treatment is paid for with less accurate information about the electromagnetic particles. Only electrons and positrons without any energy cut–off are taken into account with this option. Coordinates with arrival time, location and momenta of single electromagnetic particles cannot be obtained, but only total electron numbers at various atmospheric depths together with some parameters that give information about the general development of the electromagnetic component of a shower. At one or two observation levels lateral electron densities are computed for a grid of points around the shower axis (see below).

Longitudinal shower development

The longitudinal development of the electromagnetic part of showers is obtained by calculating the total number of electrons for ≤ 10 values of atmospheric depth separated by 100 g/cm^2 down to the lowest observation level. For each subshower initiated by gamma rays (from the π^o decay) or by electrons of energy E, the age S_i of this subshower at each interesting level i in depth z_i is calculated

$$S_i = \frac{3 \cdot z_i/X_0}{z_i/X_0 + 2 \cdot \log(E/E_{crit})} \tag{6.13}$$

with $E_{crit} = 82\ MeV$ being the critical energy and $X_0 = 37.1\ g/cm^2$ the radiation length in air. The electron number N_e of an electromagnetic subshower at the

considered depth value is then given by [59]

$$N_e = \frac{0.31}{\sqrt{\log(E/E_{crit})}} \cdot exp(z_i/X_0 \cdot (1 - 1.5 \cdot \log S_i)) \quad . \qquad (6.14)$$

At each interesting depth value, these electron numbers N_e are summed up for all subshowers.

Longitudinal age parameter

In order to describe the shower development of the overall electromagnetic or hadronic cascade in the same way as the parameter S does for individual electromagnetic subshowers, an artificial parameter, the global longitudinal age S_{long}, is introduced. Using the age parameter of eq. 6.13, the new parameters $a(S)$, $b(S)$, $C_1(S)$, and $C_2(S)$ are calculated [6]

$$a(S) = \frac{4}{S} \cdot e^{0.915 \cdot (S-1)}$$

$$b(S) = 0.15 + \frac{1}{1+S}$$

$$C_1(S) = \frac{a^{S/b}}{2 \cdot \pi} \cdot \left(\Gamma\left(\frac{S}{b}\right) + \frac{4 \cdot \Gamma(\frac{S+1}{b})}{S \cdot a^{1/b}} \right)^{-1}$$

$$C_2(S) = \frac{a^{(S+1)/b}}{2 \cdot \pi} \cdot \left(\Gamma\left(\frac{S+1}{b}\right) + \frac{4 \cdot \Gamma(\frac{S+2}{b})}{S \cdot a^{1/b}} \right)^{-1} \quad .$$

With the ratio of the coefficients $C_1(S)/C_2(S)$, the parameter R at each depth is derived by summing over all subshowers i

$$R = \frac{\sum_i (N_i \cdot C_1(S)/C_2(S))}{\sum_i N_i} \quad .$$

Finally, S_{long} is defined as

$$S_{long} = \frac{\sqrt{B^2 - 4 \cdot A \cdot (C - R)} - B}{2 \cdot A} \quad .$$

In this relation the coefficients A, B, and C depend on R and are given in table 6.3.

Lateral electron distribution

The lateral distribution of electromagnetic showers in different materials scales well with the Molière radius $r_{mol} = 21.2 \, MeV \cdot X_0/E_{crit}$. In the atmosphere X_0 varies with the density, hence, $r_{mol} = 9.6 \, gcm^{-2}/\rho_{air}$. About 90% of the energy of a shower is deposited inside a cylinder around the shower axis with radius r_{mol}. In CORSIKA the electron distribution is determined for the two lowest observation levels. The

| Range of R	A	B	C
0.0191 − 0.1796	0.3109	0.2146	-0.0055
0.1796 − 0.5364	0.3667	0.1639	0.0060
0.5364 − 1.0332	0.1460	0.6317	-0.2420
1.0332 − 1.4856	-0.3376	2.0903	-1.3438

Table 6.3: Parameters of the longitudinal age formula.

electron density ρ_e at distance r from the subshower axis is calculated according to ref. [60]

$$\rho_e = \frac{N_e}{\pi \cdot S_m^2} \cdot \frac{\Gamma(4.5 - S)}{\Gamma(S) \cdot \Gamma(4.5 - 2 \cdot S)} \cdot \left(\frac{r}{r_{mol} \cdot S_m}\right)^{S-2} \cdot \left(1 + \frac{r}{r_{mol} \cdot S_m}\right)^{S-4.5} \quad (6.15)$$

with the modulation function of Lagutin [6, 7]

$$S_m = 0.78 - 0.21 \cdot S \quad .$$

The electron densities are calculated for 80 reference points centered around the shower axis on a circular grid extending in 8 directions spaced by 45° and with 10 fixed radial distances $\leq 200m$ in each direction. The densities are summed up for each subshower and at each reference point of the grid to get the local densities of the total shower.
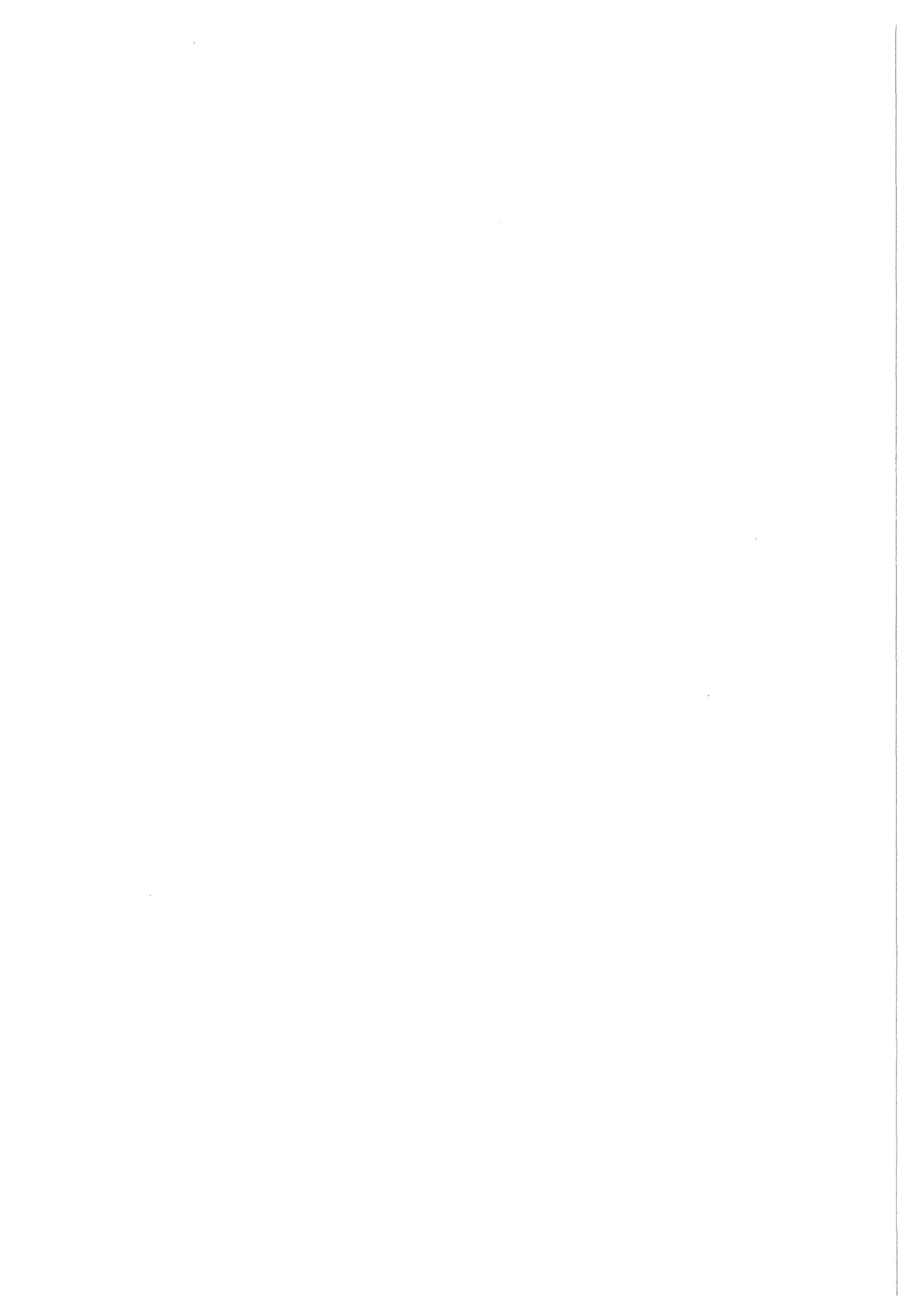
Chapter 7

Some results

In this chapter a few selected examples of CORSIKA results are shown to illustrate the agreement of the generator output with the collider results and the good global description of EAS.

7.1 Comparison of generator and data

High energy interactions simulated with the CORSIKA generator are tested by comparison with the interactions seen in collider data. In fig. 7.1 the average charged multiplicity is shown versus the cm energy as measured [37, 61, 62] and simulated by CORSIKA. The values agree well within the statistical uncertainty. In fig. 7.2
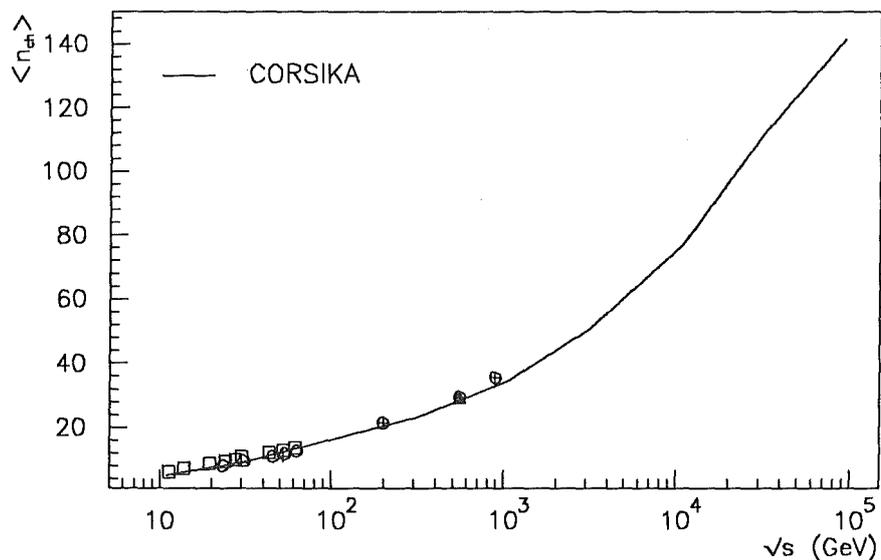
Figure 7.1: Average charged multiplicity $\langle n_{ch} \rangle$ vs cm energy. The line shows the CORSIKA results, the points give collider data [37, 61, 62].
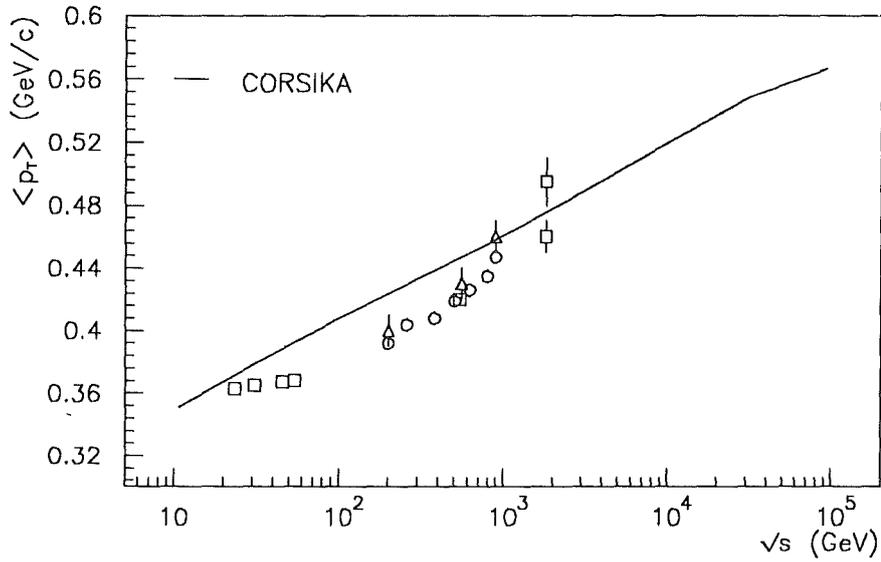
Figure 7.2: Average transverse momentum $\langle p_T \rangle$ vs cm energy. The line shows the CORSIKA results, the points give collider data [37, 63, 64, 65, 66].
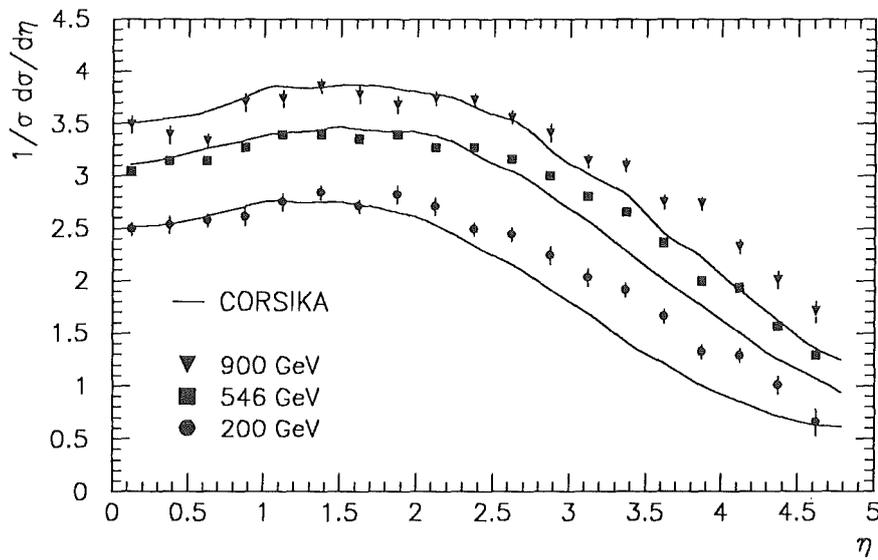

Figure 7.3: Pseudorapidity density distributions for different cm energies. The lines show the CORSIKA results, the points give collider data [67].

the average transverse momentum for pions is given versus the cm energy of the collision. The CORSIKA results and collider data [37, 63, 64, 65, 66] follow the same tendency. The simulated pseudorapidity distributions for different energies are shown in fig. 7.3 and compared with experimental distributions [67]. The variation of form and amplitude of the measured distributions with energy is well – though not perfectly – reproduced.

The general description of the high energy collisions is good and the plotted quantities follow the measured distributions of the collider data. This indicates that the boundary conditions introduced by forming one interaction out of independently modelled quantities and by fulfilling energy and momentum conservation do not lead to a major distortion of the primary distributions.

7.2 Air shower simulations

Up to now, many simulations have been performed with the CORSIKA program. Photon, proton, oxygen, and iron induced showers have been simulated in the energy range from 10^{11} eV to 10^{17} eV. For each shower all the particles arriving at an observation level with an energy above a cut–off value are recorded. From this data base a standard set of distributions is deduced. Particle numbers, energy, arrival coordinates and times, angles of incidence and particle types are plotted and
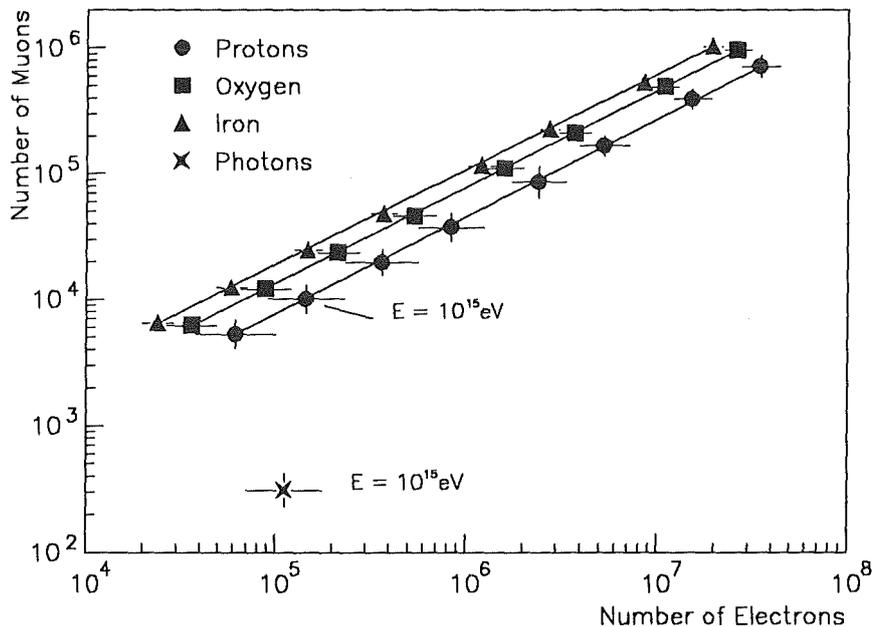

Figure 7.4: Simulated muon vs electron number for different primaries with energies of 0.5, 1, 2, 4, 10, 20, 50, and $100 \cdot 10^{15}$ eV. The error bars show the fluctuations of the plotted quantities.

analyzed. These distributions may be used to compare results of different CORSIKA versions as well as simulations and experimental data.

7.2.1 Electron and muon numbers

The number of secondary electrons N_e is usually taken to classify an EAS, because it is the quantity easiest accessible by measurement. Different primaries, however, give the same N_e at different primary energies. Additional observables are needed to resolve this ambiguity. The number of muons N_μ provides some complementary information. In fig. 7.4 N_μ is plotted versus N_e for varying primary energies and particle types as simulated by the CORSIKA program. Both, N_μ and N_e, scale roughly with the primary energy for all particle types. For fixed energy the different primary nuclei on average lie clearly apart from each other. Their fluctuations, given by the error bars in fig. 7.4, are large, especially for p induced showers, but decrease with rising energy. The N_μ values of photon showers are far below those of the nuclei and are easy to identify unless new, anomalous effects occur.

7.2.2 Single hadron spectrum

A major part of the KASCADE detector is the large hadron calorimeter [1]. This calorimeter identifies hadrons with energies above 10 GeV and, therefore, allows to measure the intensity of single hadrons. CORSIKA allows to predict the single hadron energy spectrum. The secondary hadrons with an energy E_h at sea level
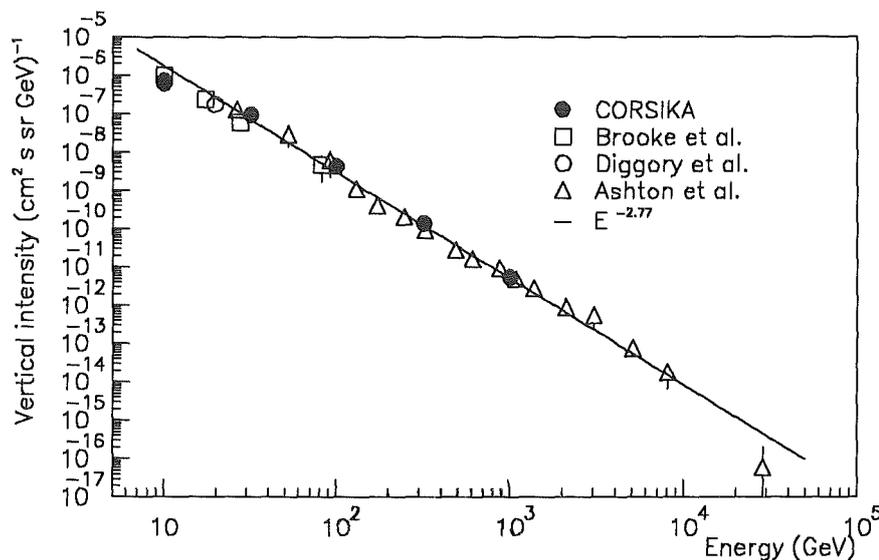

Figure 7.5: Energy spectrum of secondary single hadrons. The full dots show the CORSIKA results, the open points give various measurements [70, 71, 72]. The line represents a fit to the CORSIKA data.

originate from primaries in a wide energy range. Since low energy primaries are much more abundant than high energy ones, secondary hadrons in the energy range of 10 GeV to 10 TeV most probably come from primaries in the energy range of 100 GeV to 100 TeV. But even primaries with energies as low as $2 \cdot E_h$ contribute with a small probability. In the region from 100 GeV to 100 TeV the JACEE collaboration measured the intensities of protons and α particles [68] with good accuracy. At these energies per nucleon the abundance of heavy nuclei is below 1% [68, 69] and, therefore, can be neglected. (The energy of the secondary hadrons is determined by the energy per nucleon of the primary nucleus, rather than its total energy.) Using the JACEE fluxes for the primary particles a differential single hadron spectrum falling with $E^{-2.77}$ as shown in fig. 7.5 is obtained. It matches very well with various measurements of the total hadron spectrum [70, 71, 72, 73].

7.2.3 Mass separation

CORSIKA simulations and a subsequent detailed modelling of the KASCADE detector allow to estimate how accurately the observables of EAS can be measured in our experiment and how the individual quantities correlate with each other and the primaries' mass and energy. A multivariate analysis (Principle Component Analysis) was performed to determine mass and energy of the primary by using all information and correlations available in the shower [74]. Its result is an indicator $\lambda_E \propto E$ for the primary energy independent of the primary mass and an indicator λ_m for the primary's mass independent of the particles energy. λ_E and λ_m are linear combinations of all observables entering the analysis. For a first analysis, 7 inputs were chosen, namely the electron number N_e, the shower age S, the muon number in-
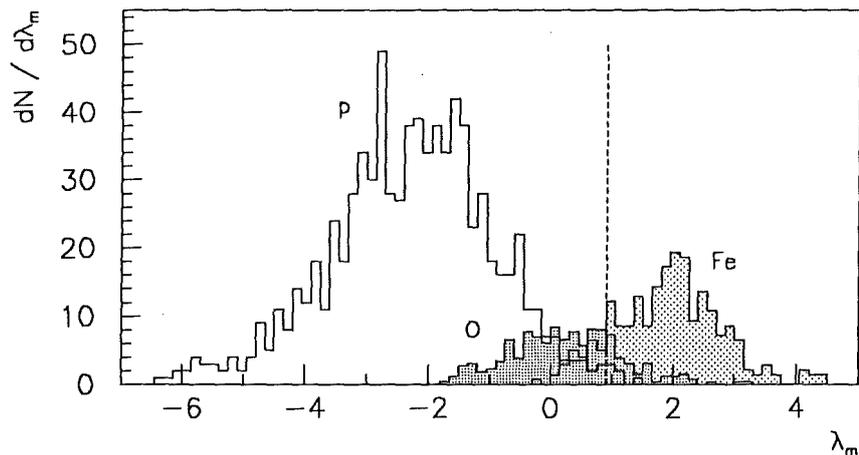

Figure 7.6: λ_m distribution for p, O, and Fe primaries. The abundance is assumed to be $p : O : Fe = 6 : 1 : 1.75$. The primary energy spectrum and the detector response are taken into account.

side 10 m core distance, the muon number inside 100 m core distance, the hadron energy sum inside 5 m core distance, the hadron energy sum inside 2 m core distance, and the maximum hadron energy. With this analysis, energy resolutions of $\sigma(E)/E = 33\%$ for proton induced showers and $\sigma(E)/E = 15\%$ for iron induced ones are achieved. These numbers already include the effects of the steep energy spectrum and the limited detector area and resolving power. The energy of protons is reconstructed systematically too high by about 14% due to the large fluctuations of proton showers, whereas for iron no shift is observed [74].

In fig. 7.6 the distribution of the mass indicator λ_m is shown for different primaries with energies varying between 0.5 and 4 PeV. The energy spectrum and the detector response are taken into account. The abundances of protons, oxygen, and iron in cosmic rays at these energies has been estimated by extrapolating the spectra measured at lower energies above the atmosphere [69]. The cut–off indicated by the straight line selects iron induced EAS with a probability of 89%, whereas only 14% of the selected showers originate from proton or oxygen primaries. The signal to background ratio is then $S/B = 6.1 : 1$. A similar analysis with N_e and N_μ only leads to $S/B = 3 : 1$.

46

Chapter 8

Outlook

The CORSIKA program in its actual state models EAS initiated by photons, protons and nuclei up to 10^{17} eV primary energy. It relies on experimental data wherever possible. CORSIKA is a useful and flexible tool to study high energy cosmic ray interactions, to support the interpretation of EAS measurements, and to optimize the design of future cosmic ray experiments.

However, the CORSIKA program is under continuous development and many details of the shower development are subject to uncertainties and approximations. Wherever we are aware of such an uncertainty, we try to improve it.

Some of the improvements to be implemented in the next future have already been mentioned in the text. They are mostly modifications to tune the interaction model as near as possible to collider results. Intermediate resonances, the manifold of secondaries, their decay modes and kinematics, distributions of energies, momenta and production angles, and correlations of the quantities may be adapted.

Unfortunately for EAS, the collider results have to be extrapolated into energy and angular regions where the interactions are supposed to change. Gluons instead of quarks become the most abundant reaction partners, heavy quarks and minijets may be produced, and the collider events might look different in the forward region compared to the region with high transverse momentum, where the collider detectors are located. Some of these extrapolations may be guided by theoretical calculations, others have to rely on intuition only.

One major effort will concentrate on improving the simulation of interactions below the DPM energy region. Here, the description is partly very general and it could be improved in many respects. A more difficult problem is the transition between the high and low energy model. Actually, in some distributions discontinuities appear due to the different philosophies of particle production below and above the transition energy.
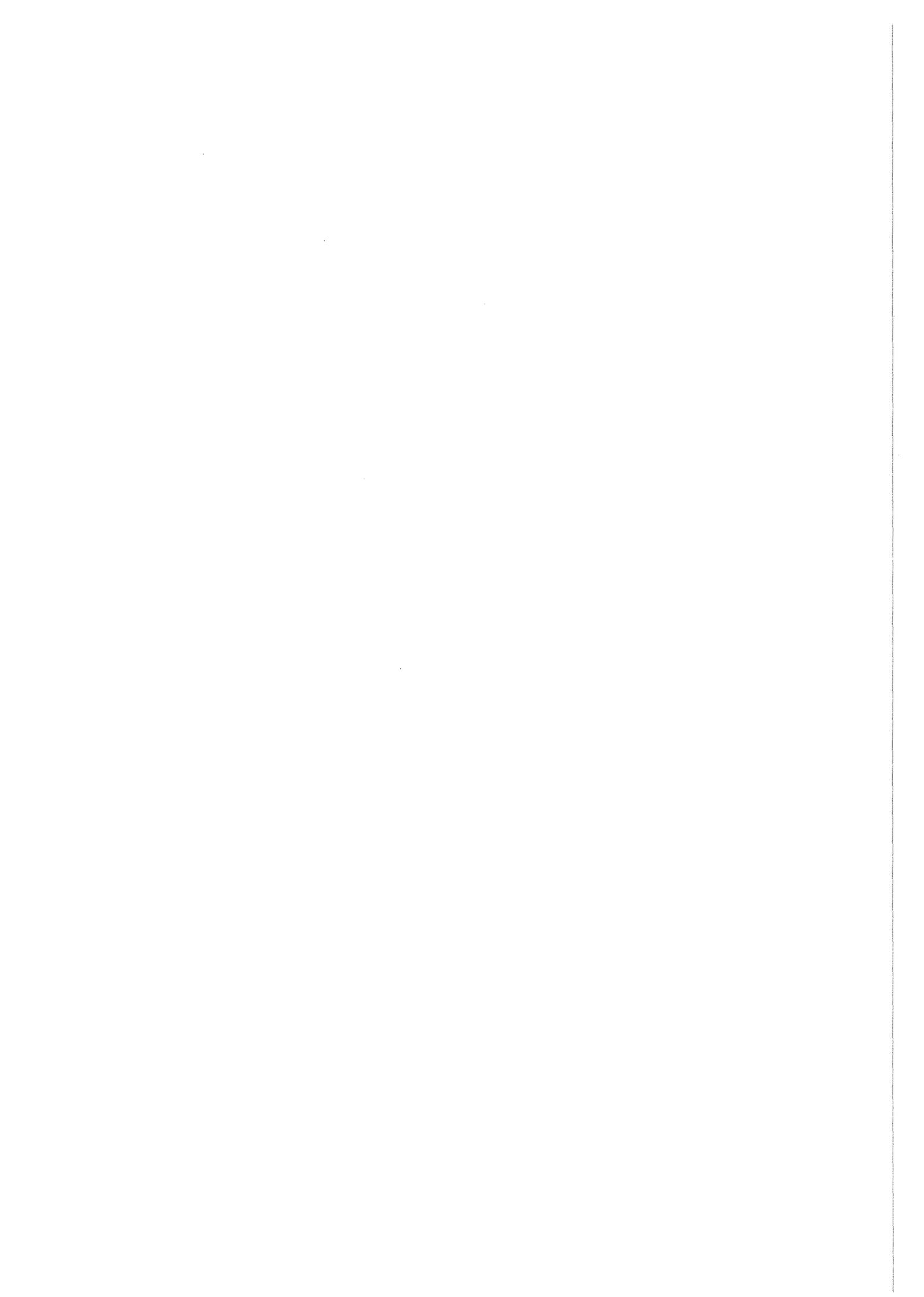
The HEGRA collaboration made an extension to simulate Cerenkov radiation [75]. This will be implemented in CORSIKA. The lateral distribution and arrival times of Cerenkov photons may then be determined at a grid of space points.

Atmospheric neutrinos optionally will be tracked down to the observation level as a further option.
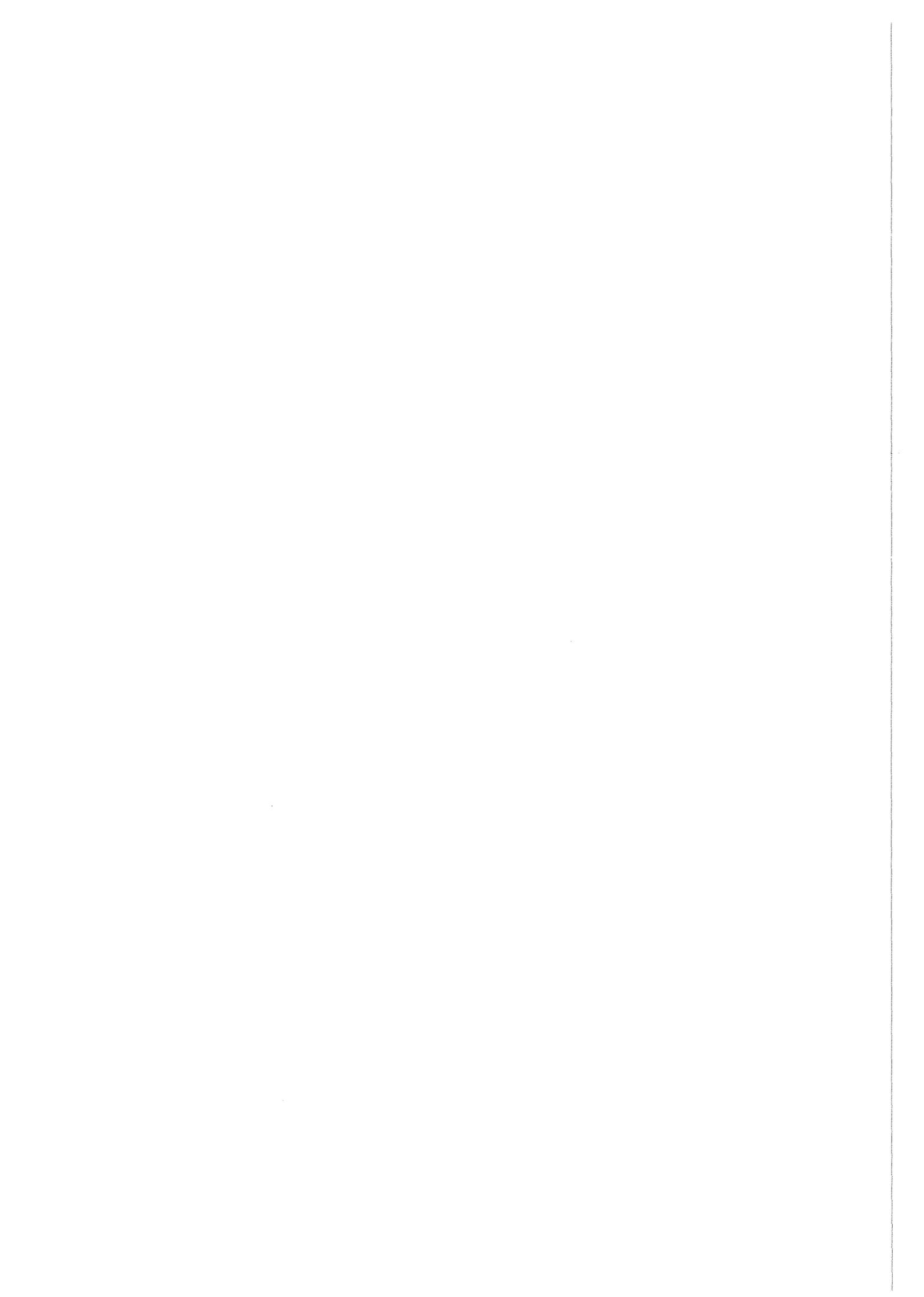
Acknowledgements

Bibliography

[1] P. Doll et al., The Karlsruhe Cosmic Ray Project KASCADE,
KfK Report 4686 (1990), Kernforschungszentrum Karlsruhe

[2] P.K.F. Grieder, Inst. for Nuclear Studies, INS–J125 (1970), Univ. of Tokyo;
P.K.F. Grieder, Proc. 16th Int.Cosmic Ray Conf., Kyoto, 9 (1979) 161

[3] J.N. Capdevielle, J.Phys.G: Nucl.Part.Phys. 15 (1989) 909

[4] A. Capella and J. Tran Thanh Van, Phys.Lett. B93 (1980) 146

[5] W.R. Nelson et al., The EGS4 Code System, SLAC Report 265 (1985)

[6] J.N. Capdevielle and J. Gawin, J.Phys.G: Nucl.Part.Phys. 8 (1982) 1312

[7] A.A. Lagutin et al., Proc. 16th Int.Cosmic Ray Conf., Kyoto, 7 (1979) 18

[8] R. Brun et al., GEANT 3, CERN Report DD/EE/84-1 (1987)

[9] Handbook of Chemistry and Physics, 65th Edition, ed. R.C. Weast,
(The Chemical Rubber Co., Cleveland, 1984) F152

[10] J. Linsley, private communication by M. Hillas (1988)

[11] G. Marsaglia and A. Zaman, Florida State University
Report FSU–SCRI–87–50 (1987)

[12] F. James, CERN Report DD/88/22 (1988)

[13] A. Baldini et al., in Landolt–Börnstein, New Series I/12 a+b
(Springer, Berlin, 1987)

[14] P. Aurenche et al., Phys.Rev. D45 (1992) 92

[15] R.J. Glauber and G. Matthiae, Nucl.Phys. B21 (1970) 135

[16] K.G. Boreskov and A.B. Kaidalov, Sov.J.Nucl.Phys. 48 (1988) 367

[17] H. de Vries et al., Atomic Nucl. Data Tables 36 (1987) 495

[18] B. Rossi, High Energy Particles
(Prentice Hall, Englewood Cliffs, New Jersey, 1952)

[19] G. Barr et al., Phys.Rev. D39 (1989) 3532

[20] T. Kinoshita and A. Sirlin, Phys.Rev. 107 (1957) 593

[21] Review of Particle Properties, Particle Data Group,
Phys.Lett. B239 (1990) VII,76

[22] Review of Particle Properties, Particle Data Group,
Phys.Lett. B239 (1990) VII,79

[23] J.N. Capdevielle, J.Phys.G: Nucl.Part.Phys. 16 (1990) 1539

[24] R.E. Ansorge et al., UA5 Collaboration, Z.Phys. C43 (1989) 75

[25] G.J. Alner et al., UA5 Collaboration, Nucl.Phys. B291 (1987) 445

[26] G.J. Alner et al., UA5 Collaboration, Phys.Lett. B167 (1986) 476

[27] J.N. Capdevielle and S. Zardan, Proc. 20th Int.Cosmic Ray Conf.,
Moscow, 5 (1987) 160

[28] K. Alpgård et al.,UA5 Collaboration, Phys.Lett. B115 (1982) 71;
G. Arnison et al., UA1 Collaboration, Phys.Lett. B122 (1983) 189;
G.J. Alner et al., UA5 Collaboration, Phys.Lett. B180 (1986) 415

[29] R.E. Ansorge et al., UA5 Collaboration, Nucl.Phys. B328 (1989) 36

[30] T. Åkesson et al., AFS Collaboration, Phys.Lett. B178 (1986) 447

[31] C. De Marzo et al., Phys.Rev. D26 (1982) 1019

[32] M. Arneodo et al., Z.Phys. C31 (1986) 1

[33] M. Aguilar–Benitez et al., NA27 Collaboration, Z.Phys. C50 (1991) 405

[34] R. Attallah et al., Proc. 22nd Int. Cosmic Ray Conf., Dublin, 4 (1991) 157

[35] R. Hagedorn, Rev.Nuovo Cim. 6 (1983) 1

[36] G. Arnison et al., UA1 Collaboration, Phys.Lett. B118 (1982) 167

[37] G.J. Alner et al., UA5 Collaboration, Phys.Rep. 154 (1987) 247

[38] J.A. Capella, Proc. 22nd Int. Cosmic Ray Conf., Dublin, 5 (1991) 15

[39] J.N. Capdevielle and T. Thouw, J.Phys.G: Nucl.Part.Phys. 18 (1992) 143

[40] R.E. Ansorge et al., UA5 Collaboration, Z.Phys. C33 (1986) 175

[41] P. Bernard et al., UA4 Collaboration, Phys.Lett. B166 (1986) 459

[42] V. Innocente et al., Phys.Lett. B169 (1986) 285

[43] J.N. Capdevielle, Proc. 5th Int.Sym. on Very High Energy Cosmic Ray Interactions, Lodz, 1 (1987)

[44] C. Geich–Gimbel, Int.J.Mod.Phys. 4 (1989) 1527

[45] J.N. Capdevielle and J. Gawin, J.Phys.G: Nucl.Part.Phys. 12 (1986) 465

[46] G. Schatz, in KfK Report 5027 (1992), eds. J.Knapp and H.Rebel, Kernforschungszentrum Karlsruhe, p.32

[47] A. Klar and J. Hüfner, Phys.Rev. D31 (1985) 491

[48] A. Capella, LPTHE Orsay Report 91/53 (1991)

[49] T. Åkesson et al., HELIOS Collaboration, Z.Phys. C49 (1991) 355

[50] G. Schatz and D. Heck, in KfK Report 5027 (1992), eds. J.Knapp and H.Rebel, Kernforschungszentrum Karlsruhe, p.35

[51] P. Blüm et al., Kernforschungszentrum Karlsruhe (1988), unpublished results

[52] R. Hamatsu et al., Nucl.Phys. B123 (1977) 189

[53] D. Everett et al., Nucl.Phys. B73 (1974) 440

[54] T. Stanev et al., Phys. Rev. D32 (1985) 1244

[55] F. Eisele and G. Wolf, Phys.Bl. 48 (1992) 787

[56] H. Genzel et al., in Landolt–Börnstein, New Series I/8 (Springer,Berlin, 1973)

[57] R.M. Sternheimer et al., Phys.Rev. B26 (1982) 6067

[58] J. Spitzer, private communication (1988)

[59] K. Greisen, Prog. Cosmic Ray Physics Vol. III, (North Holland Publishing Co., Amsterdam 1956)

[60] M.F. Bourdeau et al., J.Phys.G: Nucl.Phys. 6 (1980) 901

[61] W. Thomé et al., Nucl.Phys. B87 (1975) 41

[62] R.E. Ansorge et al., UA5 Collaboration, Z.Phys. C43 (1989) 357

[63] C. Albajar et al., UA1 Collaboration, Nucl.Phys. B335 (1990) 261

[64] A. Breakstone et al., Z.Phys. C33 (1987) 333

[65] T. Alexopoulos et al., E737 Collaboration, Phys.Rev.Lett. 60 (1988) 1622

[66] F. Abe et al., CDF Collaboration, Phys.Rev.Lett. 61 (1989) 1819

[67] G.J. Alner et al., UA5 Collaboration, Z.Phys. C33 (1986) 1

[68] T.H. Burnett et al., Astroph.J. 349 (1990) L25

[69] D. Müller et al., Astroph.J. 374 (1990) 356

[70] F. Ashton and A.J. Saleh, Nature 256 (1975) 387

[71] G. Brooke and A.W. Wolfendale, Proc.Phys.Soc. 83 (1964) 843

[72] I.S. Diggory et al., J.Phys.A: Math.Nucl. and Gen.Phys. 7 (1974) 741

[73] M. Nieminen et al., J.Phys.G: Nucl.Part.Phys. 11 (1985) 421

[74] P. Gabriel, KfK Report 5012 (1992), Kernforschungszentrum Karlsruhe

[75] HEGRA Collaboration, CORSIKA Workshop, Karlsruhe 1991, (unpublished)